Abdullahi, A.A., Nahar, N., Azuddin, M., and Choudhury, I.A. (2017) Net-Shape Microfabrication Technique by Micrometal Powder Injection Molding. In: Hashmi, M.S.J. (ed.), Comprehensive Materials Finishing. vol. 1, pp. 466–503. Oxford: Elsevier.

1.16 Net-Shape Microfabrication Technique by Micrometal Powder Injection Molding

AA Abdullahi, University of Malaya, Kuala Lumpur, Malaysia and Federal University of Technology, Minna, Nigeria
N Nahar, M Azuddin, and IA Choudhury, University of Malaya, Kuala Lumpur, Malaysia

 doi:10.1016/B978-0-12-803581-8.09162-1

1.16.1 Introduction

Net-shape microfabrication of parts and components by powder injection molding (PIM) is classified into metal injection molding (MIM) and ceramic injection molding (CIM) processes. The technology of CIM has been around since the 1940s for fabrication of parts and components from ceramic powders such as titania, alumina, zirconia, ferrite, and others. However, the invention of MIM is believed to have been developed in the United States in the 1970s by Raymond E. Wiech. The PIM offers significant advantages over other microfabrication techniques. These include cost-savings, increased flexibility in design and materials, increased possibility of miniaturization, shape complexity, good surface finish, dimensional accuracy, and high mechanical properties of molded parts.[1–5] These attributes placed PIM over other microfabrication techniques such as micromachining, laser ablation, hot pressing, investment casting, and etching. PIM involves process integration of the flexibility and design of plastic injection molding with excellent material properties of powder metallurgy for metals and ceramics powders for molded parts. There are four processing steps: feedstock preparation (mixing of the ceramic or micrometal powder and binder constituents); injection molding of the feedstock to produce the desired shape; debinding; and sintering of the green and brown parts, respectively. However depending on the application or requirements specifications of the part, postprocessing such as heat treatment, hot isostatic pressing (HIP), machining, or surface finish improvement are sometimes performed, especially for the automotive, medical and aerospace parts fabrication. PIM has been found to be very efficient and cost-effective in the manufacturing of a wide range of products such as automotive parts, mobile phone components, surgical instruments, medical implants, microfluidic components, electronics components, and sport equipment. These successes were achieved based on the principles of convectional or plastic injection molding processes, but PIM was adopted mainly for material properties and service condition improvement.

The plastic injection molding is the most versatile process for the manufacturing of plastic products. It continues to be the process of choice for the production of parts with complex three-dimensional (3D) shapes. The technology has been successfully used to produce parts based on composites, foams, rubber, and thermosets, in addition to thermoplastics. These developments in the convectional injection molding process have extended the technology in recent years to covered PIM. Likewise, special cases of inventions and innovations have been incorporated into the process to improve the efficiency and versatility of the process and products. In the past few years, several types of IM processes have been developed, such as micropowder injection molding (μPIM), low-pressure injection molding (LPIM), water-assisted injection molding (WAIM), microsacrificial plastic mold insert MIM (μSPiMIM), microinjection molding, bicomponent injection, multishot injection molding, and co-powder injection molding (2C-PIM).[6] In addition, developments in instrumentation and control facilities of the machine through installation of thermocouples, pressure transmitters, valves, controllers, and sensors are ongoing to achieve the best quality product as the process increased in production of miniaturization parts.

Decreases in micro-size channels of mold cavities and part dimensions brought about technical challenges that affect molded part quality. However, μIM is more than downsizing of machine parts dimensions and requires rethinking of the entire process for its success. Therefore, as the machine size is reduced, the process is associated with part defects. Defects occur such as incomplete filling of mold cavity, sink marks, part deformation or distortion, and cracks, which are more visible at debinding and sintering stages. Similarly, nonhomogeneity or segregation of powder-binder particles during the mixing stage has been a challenge in PIM.[7–10] However, these challenges are minimized through optimization of the PIM process and focusing on some selected processing parameters that enhance a defect-free part. Performance and product quality are enhanced by optimization and modeling of the processing steps of μIM. Meanwhile, to produce parts or components with high quality and a low rejection rate, a comprehensive understanding of the entire production process is required, along with the development of appropriate quality monitoring and process-controlled systems or framework. This framework is expected to cover the whole PIM process chain, from feedstock preparation to finished part. There are a number of processing steps whereby a small change will directly influence manufacturing tolerances and material properties of the finished part.

Therefore, this chapter presents an overview of μPIM as a net-shape microfabrication technique, with special attention given to the micrometal injection molding (μMIM) process. Brief descriptions of the equipment, principles, and processing steps of injection molding for defect-free products (feedstock, green part, brown part, and finished part) are presented. Furthermore, optimization and simulation of the μIM, part fabrication, and various applications of PIM are discussed.

1.16.2 Injection Molding Equipment

Injection molding technology can be linked to the invention of John and Isaiah Hyatt in the year 1872. They were the first to patent the injection molding machine (IMM). This machine is designed to inject the plastic melt through a heated barrel

into the mold cavity. It is referred to as stuffing plunger IMM.[11] However, the industry has been developing progressively; nevertheless, in 1946, the industry witnessed a complete turnaround from the earlier design to the first screw IMM by James Watson Hendry. The screw design concept now dominates the commercial IMM. Due to process development, the design is further expanded to handle multishot, bicomponent, and multicomponent injection molding at macroscale and microscale. In addition, the custom-made IMM are developed by researchers and research group(s), including manually operated machines and electric-driven, pneumatic, and hybrid types, respectively. According to Chang *et al.*,[12] the commercial IMM are mostly electric-hydraulic hybrid types or fully electric types. A market survey shows that commercially available IMM are produced by Ferromatik Milacron, Arburg, and Sumitomo Demag. However, Wittmann-Battenfeld, Babyplast, and Desma are known manufacturers of the microinjection molding machine (μIMM). The improvements of the screw-over-plunger design are the incorporation of and modification to the plastification units and control system features of the IMM to enhanced μIM.

In addition, to make the technology more accessible and affordable, especially for small and medium manufacturing enterprises (SMEs), researchers still embark on the development of manually operated IMM. There is a remarkable record of US patents[13–17] for the development of hand-operated IMM and μIMM[18–20] systems. However, some other pieces of equipment are required to effectively perform injection molding tasks. These tools include the feedstock mixing mechanism/machines, IMM, and debinding and sintering apparatuses. Therefore, the next subsection focuses on discussion of the apparatus for processing steps of μIM.

1.16.2.1 Feedstock Mixing Mechanism

Preparation of PIM feedstock is performed by high-shear mixers that operate based on either the batch type or continuous type. In addition, well dispersive and distributive mixing of powder-binder particles is desired to create homogenous feedstock. The operation comprises everything from premixing of metal powders and polymeric binder constituents to compounding of the feedstock. A variety of compounding equipment such as single screw, twin screw, multiscrew extruder, cams, banbury, rollers, Z-blade, and double planetary mixer, among others, are adopted for the design of various mixing mechanisms. The twin screw extruder has been the most successful because it combines high shear rate and short dwell time at high temperatures. However, the cost of the twin screw extruder is high. The double planetary mixer is mostly preferred because it provides a good balance of cost, quality, and productivity.[21] However, further process developments to enhance feedstock mixing mechanism have been investigated over the years. For instance, a relatively new mixing mechanism that has been developed is based on shear roll extrusion. A pair of parallel rolls with helical grooves are heated and rotated as the powder-binder composite is fed on one roll. The gap between the roll is usually 5–7 mm, although a special arrangement of the rolls can be made for possible adjustments. The feedstock is finally extruded from the chamber and shredded.

A survey of literature shows that four types of mixing mechanisms are commonly used for preparing PIM feedstock. These mixing mechanisms are high-shear mixers, roll mills, screw extruders, and shear rolls.[22] The first two are examples of batch operations, whereas the last two are continuous. Feedstock homogeneity is an important factor that determines performance of the mixing mechanism and a better molded part by IMM.

1.16.2.2 IMM

A typical IMM is composed of plasticating, injection, mold, mold clamping mechanism, and control units, respectively. It is important to note that plastic and metal powder IMM both operates on the principle of forming produced parts and components. But a pronounced difference exists in the injection unit and control system. Therefore, based on structural arrangement of the machine components, IMM is classified as horizontal, vertical, and hybrid types, as illustrated in **Figure 1**.

i. Horizontal IMM: This is when both injection and clamping units are combined or arranged horizontally. The clamping unit is usually located on the left side of the machine.
ii. Vertical IMM: When both injection and clamping units are combined or arranged vertically. The clamping unit is usually located at the bottom of the machine.
iii. Hybrid IMM: In many situations, this is when the design combines both vertical clamping and horizontal injection units or otherwise utilizes and enhances productivity. Combination of one injection and one clamping unit is common. However, multiple units, such as two injection units and one clamping unit, are utilized for multicolor and/or bicomponent injection molding. Recently, some machines have been built to perform two-color injection machines, rotary injection machines, low-foam injection machines, multimaterial injection machines, and sandwich injection machines.

However, based on the system drive, IMM is classified as hydraulic type, pneumatic type, electric type, and hybrid type, which usually involves a combination any of the drive systems.

Based on the plasticating and injection medium, it is classified as the plunger type and reciprocating screw type, which can be further classified as the screw preplasticizing and in-line screw design, respectively. **Figure 2** shows the schematic representation of the IMM based on the injection and plasticating unit of IMM.[23]

The plunger type is simple and usually adopted in a custom-made IMM. The commercial IMM utilizes the screw type or hybrid (a combination of the screw and the plunger type). **Table 1** presents a list of some available μIM machines and their specifications.

In **Table 1**, the companies that still produce the plunger-type IMM are Lawton, Desma, and Babyplast; however, some hybrid design by Wittmann-Battenfeld, Nissei, Sodick also exist. It is observed from the available statistics that the screw-type IMM now dominates the market.

Records have shown that in 1957, the first in-line screw-type IMM was developed at Ankerwerk Corporation of Germany. This machine is built with the capability of combining two processes (plasticization and injection). However, before

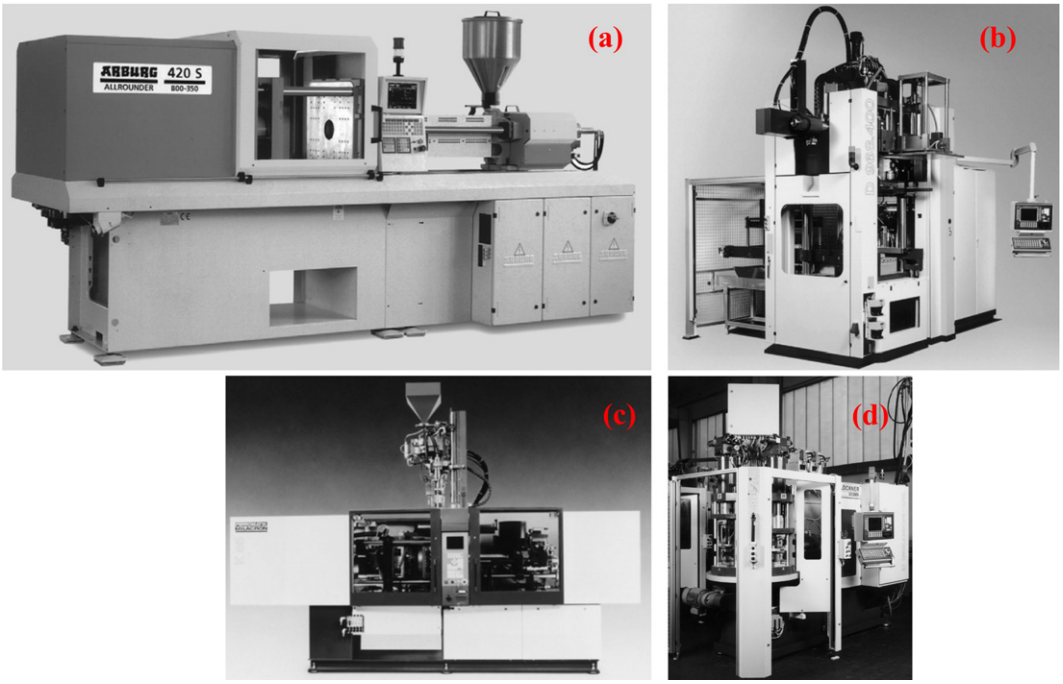

Figure 1 Basic types of injection molding machine based on structural components arrangements: (a) horizontal IMM; (b) vertical IMM; (c) hybrid-featuring two-component IMM by Ferromatik Milacron; and (d) rotary table IMM. Walter, M.; Helmut, G.; Gernot, K.; Frank, E. Lesson 2: The Injection Molding Machine. In *Training in Injection Molding*; Carl Hanser Verlag GmbH & Co. KG, 2001; pp. 19–30.

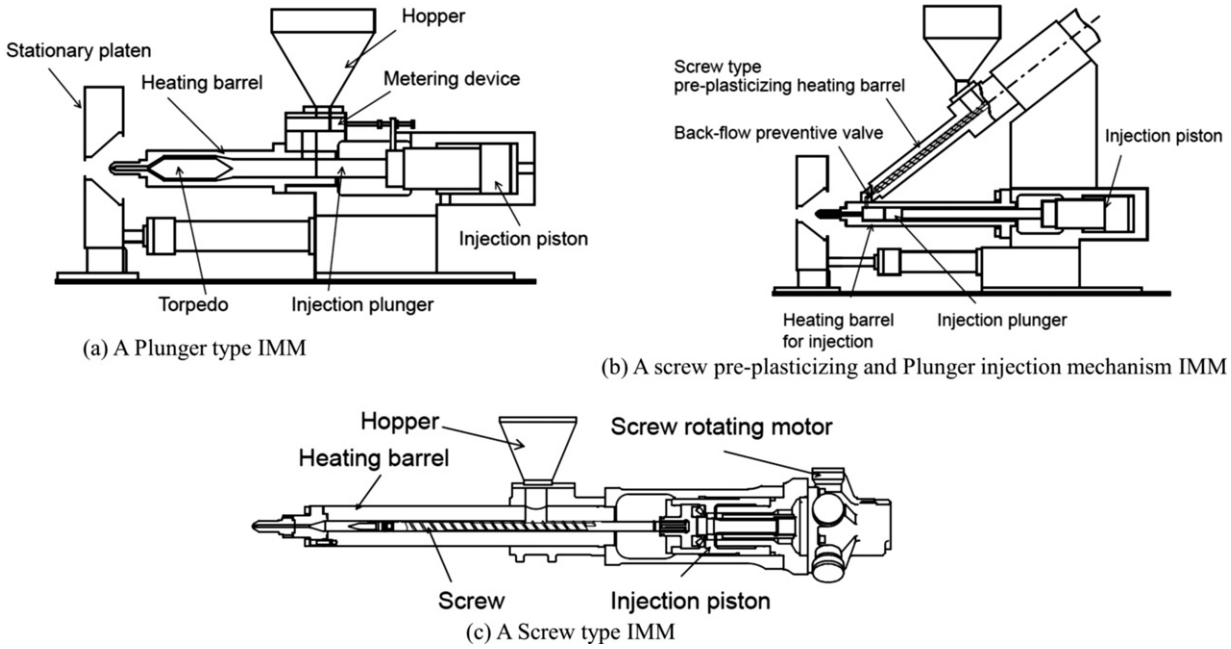

Figure 2 Schematic representation of the IMM based on injection unit. Sakai, T.; Kikugawa, K. Part II: Injection Molding Machinery and Systems: Injection Molding Machines, Tools, and Processes. In *Injection Molding*; Kamal, M. R., Isayev, A. L., Shih-Jung Liu, Eds.; Hanser, 2009; pp. 71–131.

the invention of the in-line screw-type design, the plunger or preplasticization type had been in the main stream. However, the in-line screw-type design has some demerits, such as low plasticizing capacity, poor kneading, high pressure drop during injection process, and thermal degradation by stagnation in the plunger zone.[23] The screw-type design of IMM consists of the plasticating unit melting, mixing, and conveying the molten feedstock into the mold cavity to produce the desired shaped part. Therefore, for a typical reciprocating screw IMM, special attention is given to the screw design, the mold cavity

Table 1 Commercially available μIM machines and their specifications

Manufacturer	*Model name*	*Max. clamping force (kN)*	*Theoretical injection volume (cm3)*	*Max. injection pressure (MPa)*	*Screw (S) or piston (P) diameter*[a] *(mm)*	*Max. injection velocity (mm s^{-1})*
Lawton	Sesame nanomolder	13.6	0.082	350	P10	1200
Desma	FormicaPlast	100	0.15	300	P6/P3	500
APM	SM-5EJ	50	1	245	S14	800
Wittmann-Battenfeld	MicroPower 5	50	1.2	300	S14/P5	750
Nissei	AU3E	30	1.4	250	S14/P8	300
Sodick	LP10EH2	100	2	197	S14/P8	1500
Babyplast	Babyplast 6/10P	62.5	4	265	P10	–
Rondol	High force 5	50	4.5	160	S20	–
Boy	XS	100	4.5	313	S12	–
Toshiba	EC5-A	48	5.6	200	S14	150
Fanuc	Roboshot S2000-I 5A	50	6.0	200	S14	300
Sumitomo (SHI) Demag	SE18DUZ	170	6.2	223	S14	500
Arburg	220S	150	15	250	S15/S8	112

[a]A/B = Plasticization unit/injection unit.

design, and the clamping units because they affect the quality of finished parts.

1.16.2.2.1 Screw design for IMM

The screw design of IMM is characterized by three distinct zones along the length (L). These zones are the feeding zone, compression (transition) zone, and metering zone, respectively The feed zone conveys the powder-binder composite fed through the hopper to the compression (transition) zone of the screw. This section of the screw is usually designed with a variable depth, whereas the other sections are based on constant depth. The change in this section of the screw is an important factor that influences compression. The screw geometry is normally tapered, especially for the transition zone. The compression forces on the powder-binder composite cause feedstock melt through high shear between the screw element and the walls of the barrel as well as the interaction between the molecules of the feedstock. Thereafter, the melt is conveyed to the metering zone, which ensures accumulation of enough shot volume to be injected into the mold cavity.

However, it is important to note the selection of the appropriate screw design configuration, with the shot volume matching well with the plasticizing capacity. Otherwise, gas bubbles due to excessively long residence time and design geometry mismatch are likely and may lead to binder degradation. Therefore, the design parameters such as the compression ratio (CR) and the ratio (L/D) of the screw length (L) and the diameter (D) and various depths of full-flight screws are considered and expressed as:

$$\text{Compression ratio (CR)} = \frac{\text{Channel depth in feed section } (h_f)}{\text{Channel depth in metering section } (h_m)} \quad [1]$$

$$\text{Length} - \text{over} - \text{diameter } (L/D) = \frac{\text{Screw flighted length } (L)}{\text{Screw outside diameter } (D)} \quad [2]$$

Typically in injection molding, the CR ranges from 1.8 to 2.2, and the ratio between the screw length, L, and the diameter, D, (L/D) is 18–22. In general, longer L/D of the screw length allows higher melting and mixing performance. The screw diameter is important because it determines the maximum available injection pressure. It is inversely proportional to the pressure available: the smaller the diameter, the higher the available pressure. Second, the screw diameter is a major factor that determines the maximum shot size, but a direct relationship exists between the screw diameter shot size. Researchers have investigated the performance of the screw design in injection molding in terms of product quality characteristics, such as the degree of distributive and dispersive mixing of the composite feedstock matrix, increase in plasticating capacity, and feedstock melt homogeneity. Details of the screw design and performance evaluation for injection molding are presented by Verbraak and Meijer.[24] Their study investigates the effects of the screw zone on the performance of the plasticating feedstock homogeneity, which is a prerequisite for achieving high-quality molded parts as the melt is injected into the mold cavity.

1.16.2.2.2 Mold design

The mold is sometimes described as the heart of the IM process. This is because its design, features, and condition directly influence the quality of the molded part. This important unit of IMM provides several functions such as: enclosed cavity for the melt to replicate the features and/or for configuration of the part design; solidification of the material; cooling of the material; venting of entrapped air; and ejection of the parts. Therefore, the mold design in the injection molding process has been identified among the critical factors influencing the finished part quality. **Figure 3** shows broad classification of mold design categories used for injection molding.

The common types (two-plate, three-plate) and special types (slide, slit, stripper, screw, and others) are available in commercial IMM. However, the simplest and dominant mold

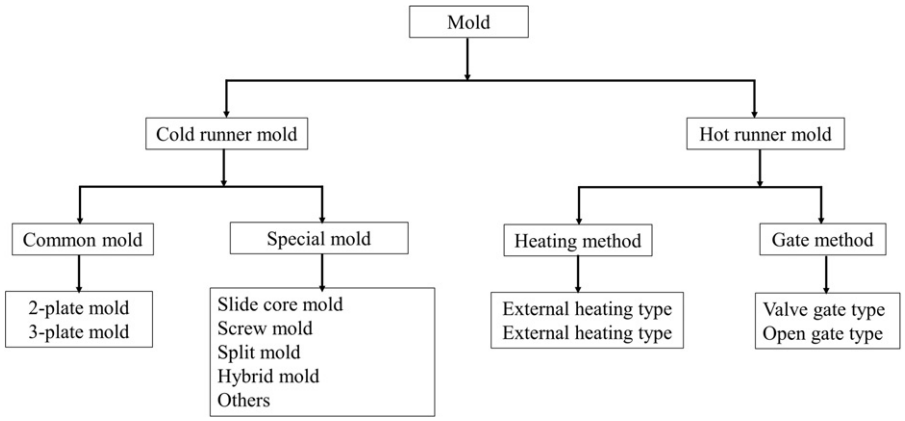

Figure 3 Classification of mold design for injection molding machine.

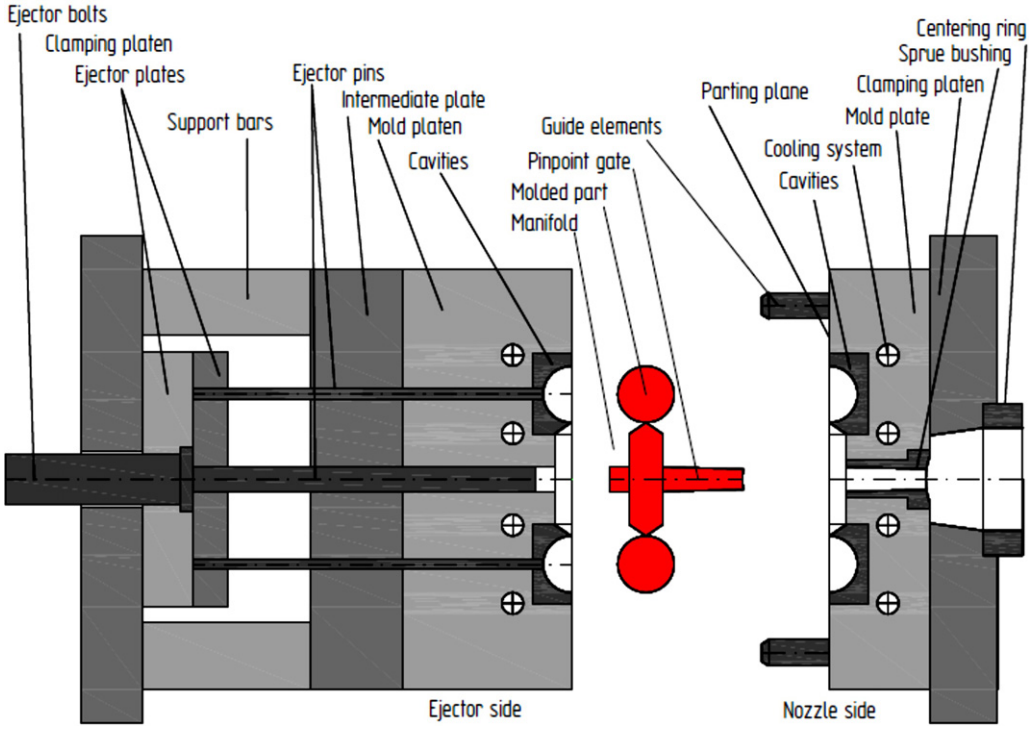

Figure 4 Typical feature of a two-plated mold.

design utilizes the two-plate design, especially for custom-made machines. A typical two-plate mold is design to have two halves, a nozzle side, and an ejector side, respectively. Figure 4 illustrates the cavity inserts, the sprue systems, the cores, the ejector elements (such as ejector pins, ejector plates, and guide element), and the cooling system, which are shown in the mold halves, respectively. In general, it is important to note that in injection molding, a mold is composed of five important parts/components:

- center ring and other mounting components for the connecting mold on IMM;
- mold cavity/cavities pattern representing the molded part design;
- runners, sprue, and gates for delivery of melt to mold cavity;
- cooling system path for cooling molded part and;
- ejection mechanism for the ejecting molded part.

The mold designer attributes special consideration to the shrinkage, which may affect the molded part from design stage, although part shrinkage is noticed after sintering. Therefore, the mold designers empirically predict the linear shrinkage (δ) of the molded part (for instance, a rectangular bar) using eqn [1], expressed as:

$$\delta = \frac{L_0 - L}{L_0} \times 100 \qquad [3]$$

The ratio of the mold cavity (L_0) and final part (L) dimensions are expressed as tool cavity expansion factor (Z).

$$Z = \frac{L_0}{L} \quad [4]$$

Likewise, Z can be expressed in terms of shrinkage as:

$$Z = \frac{1}{1-\delta} \quad [5]$$

However, it is important to note that the linear shrinkage (δ) is related to the mold cavity dimension and is usually larger than the final sintered part dimension as it relates to the tool cavity expansion factor (Z). In addition, fine-tuning of the mold cavity dimensions becomes necessary for close dimension and tolerance of the part. Then, polishing of the mold cavity becomes necessary to achieve a high-quality molded part. Polishing of the mold cavity is time-consuming, but very important, because it directly affects molded part quality in terms of the surface finish. Many researchers have devoted time to investigating mold design and fabrication to increase the competitiveness required for overall optimized manufacturing processes of IM. The finishing process of the mold is typically composed of an accurate milling stage to manage shape deviations, followed by polishing operations to achieve the required surface finish. However, local improvements of milling and the polishing set independently do not necessarily lead to optimal manufacturing process planning.[25–28] A polished, smooth mold cavity improves the flowabilty of the melt within the cavity as the it is fed through the sprue, runner, and gate. Therefore, the design of these features is very important.

1.16.2.2.3 Runner and gating system design

The structure of the mold encloses cavities, among which are the runner, gate, core cavity with features of the part to be molded, and the cooling channel. Therefore, appropriate location of the gate and runner system design for hot melt and cooling medium (usually water, ethylene glycol, blend of ethylene glycol/water, oil, and coolanol 25:chevron, etc.) are important factors considered during mold design in the injection molding process.

A typical runner system in IM is a micro-size channel that directs the melt flow from the sprue to the mold core cavities. The design of a sprue is a conical-shaped channel of typically approximately 6 mm in diameter and tapered 5°; it conveys the melt to the mold cavity with high pressure. It is important to note that high pressure is required to push the melt through the path or micro-size channel system during the filling phase of the mold cavity. As the melt flows through the runner system, frictional and heat energy are generated within the melt. Therefore, attention is given to runner dimensions. Large-dimension runners facilitate the flow of melt material at relatively low pressure. However, such designs require a longer cooling time, more material consumption, and high clamping force. Therefore, there is a need for an optimum design that will maximize efficiency for both raw material use and energy consumption during the injection molding process. Determination of the optimum runner size dimension is a serious challenge because the pressure required may be insufficiently supply by the molding machine capacity. The three basic types of runner system designs used in injection molding are illustrated in Figure 5.

The 'H' (branching) and radial (star) systems are considered to be naturally balanced runner systems. A runner is said to be balanced when it provides equal distance and runner size from the sprue to all the cavities, so that each cavity fills under the same conditions. Although the standard (Herringbone) runner system is naturally unbalanced, it can accommodate more cavities than its naturally balanced counterparts, with minimum runner volume and less tooling costs. However, an unbalanced runner system can be artificially balanced by changing the dimensions (diameter and the length) of the runner, and sometimes the cavity layout is involved.

The number of cavities in a mold plays a significant role not only for the efficiency of the molding process but also for the quality of the injection-molded parts. The artificial balancing of the standard (herringbone or in-line) runner system is highly recommended. A symmetrical runner system with H-branching or T-branching is used to correct the unbalanced runner system. The possible numbers of cavities resulting from the symmetrical runner alignment are 2, 4, 8, 16, 32, 64, 96,

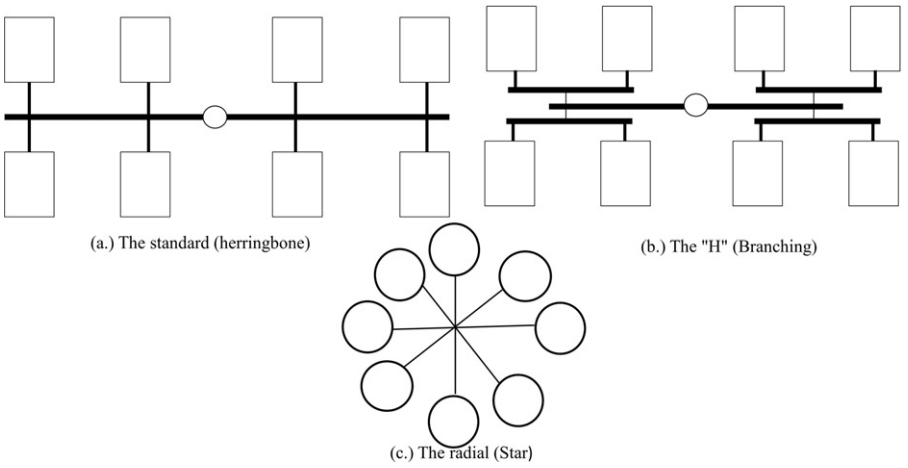

Figure 5 The basic runner design system used in injection molding.

128, and so on. Mold designs with 10, 14, 20,… cavities are not recommended. However, simulation software such as C-Mold, Moldflow, and Solidworks plastics are now available for mold filling analysis with the capability of handling mold balancing. Although, as stated previously, a runner system is artificially balanced by changing the dimensions (diameter and the length) of the runner.

In the injection molding process, the melt is transported from the plasticizing unit to the cavity through runner and gate systems. Small or micro-size runners and gates are needed in the micromolding process because the process targets meso-components and microcomponents. The melts are subject to very high shear rates during flow through the runner to the gate systems and eventually to the mold cavity. Although the effects of such severe processing conditions on the functionality and longevity of final components are yet to be addressed, flow behavior of the melts will certainly be affected by the runner and gate designs. An estimate of the wall shear rate in a circular cross-section channel is evaluated by the following relationship:

$$\dot{\gamma}_w = \frac{32Q}{\pi d^3} \quad [6]$$

where $\dot{\gamma}$ is the wall shear rate, Q is the volume flow rate, and d is the diameter of the flow channel. Because volume flow rate is a function of the injection speed and the injection plunger diameter in a plunger injection process, eqn [6] can be rewritten as the lens array

$$\dot{\gamma}_w = \frac{8VD^2}{d^3} \quad [7]$$

where D is the injection plunger diameter and V is the plunger injection speed. The shear rate in a runner is therefore a function of the injection speed, plunger diameter, and the size of the runner system. Similarly, the injection gate sizes must be related to the part dimensions.[29] The injection gate size can be determined with the following semi-empirical relationship, expressed as:

$$R = \left[\frac{3n+1}{2\pi(2n+1)} \cdot \frac{V}{NL} . h^{\frac{n+1}{n}}\right]^{\frac{n}{3n+1}} \quad [8]$$

where R is the gate radius of the injection point, n is the power law index (representing the shear thinning behavior of melt), V is the part volume, N is the number of injection gates, L is the part length, and h is the part thickness.

1.16.2.2.4 Part design for micro-PIM

A good part design in μPIM is an important aspect for the success of the process. However, most of the literature is based on individual case studies that are intended for lab-based prototyping, and no comprehensive design rules have been set for the design of microcomponents in μPIM. This situation necessitates a common concern among several active research groups of μPIM because part design information is poorly documented and comprehensive case studies are not readily available.[2]

It is important to note that most μPIM parts are small, complex, thin-walled, and (like Goldilocks) 'just right,' with neither too few nor too many features. Some typical attributes of parts fabricated by μPIM are[30]:

- mass is approximately 10 g, but the range is from 0.02 to 500 g
- maximum dimension is 25–35 mm, ranging up to 260 mm
- wall thickness often is 2–3 mm, ranging down to 0.1 mm.

In addition, Table 2 presents a typical collection of some variations observed in parts and/or components designed for microfabrication by μPIM. Although these quantities are relative to the specified feature and the actual values encountered in production depend on many factors, researchers strive for alternatives and continuous improvements of quality parts.

1.16.2.2.5 Clamping unit

The clamping mechanism of the IMM is either hydraulically or mechanically actuated. In industry, the capacity of the clamping unit is used as the measure for the determination of the size of the IMM. In addition, the clamping mechanism is a major cost factor considered for selecting IMM. In general, there are two main functions performed by the clamping unit during the molding process. It provides the required sufficient clamping force on the mold during injection of feedstock into the mold cavity and subsequent packing phase. The opening and closing of the mold are usually handled by the clamping unit.

1.16.2.3 Auxiliary and Other Equipment for Injection Molding Process

The support of other pieces of equipment is necessary in some cases and other processing steps of IM. These pieces of tooling are termed auxiliary equipment for their various supporting functions. Table 3 outlines some auxiliary equipment used in the IM process.

In addition, other pieces of equipment such as the solvent debinding system and heat furnace are required for solvent debinding and thermal debinding as well as the sintering process.

Table 2 Typical variations observed in parts design for fabrication by μPIM

Part feature	*Tolerance (±)*	
	Typical	*Best possible*
Angle (°)	2	0.1
Density (%)	1	0.2
Weight (%)	0.4	0.1
Dimension (%)	0.3	0.05
Absolute dimension (mm)	0.1	0.04
Hole diameter (%)	0.1	0.04
Hole location (%)	0.3	0.1
Flatness (%)	0.2	0.1
Parallelism (%)	0.3	0.2
Roundness (%)	0.3	0.3
Perpendicularity (%)	0.2	0.1
Perpendicularity (°)	0.3	0.1
Average surface finish (μm)	0.8	0.4

Table 3 Auxiliary equipment and application

S.no.	*Equipment*	*Purpose/function*
1	Dryer: Oven (drawer or tray) dryers, hopper dryer, and floor (Central) dryer	Required/used when the feedstock is made from hygroscopic binder systems
2	Loader: Mechanical loader, vacuum loader, and positive-pressure loader	Act as storage and feeding mechanisms of feedstock into injection molding machine
3	Blender: Manual blending, machine-mounted blender	Required for premixing of the metal powder and/or the binder components, followed by compounding process
4	Granulators	A system that grinds scrap parts, thereby producing granule-size feedstock for reuse
5	Mold temperature controllers	To maintain mold temperature, mostly used for feedstock that requires close monitoring because it also circulates the cooling fluid via the mold cooling route or path
6	Robots	Used in performing tedious, repetitive control and monitoring of molding operations

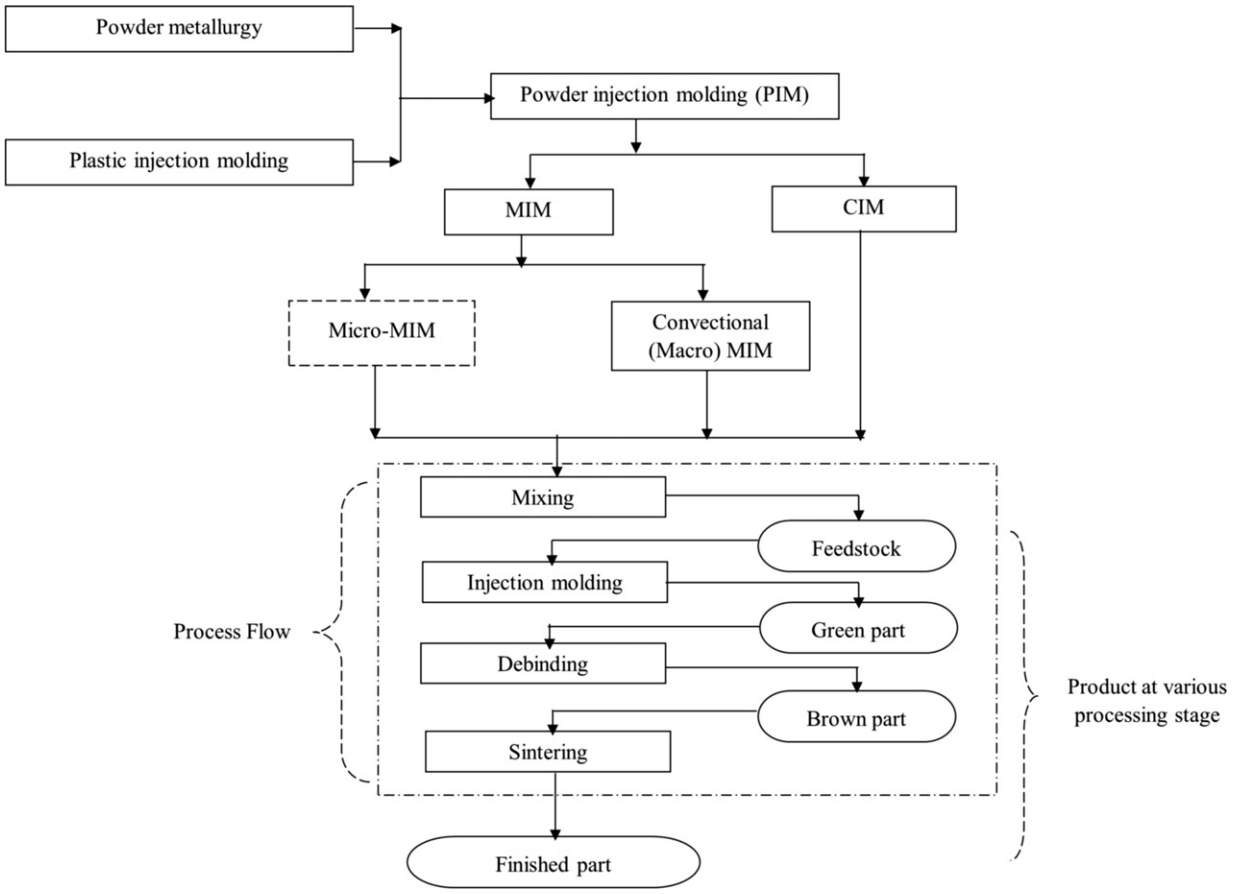

Figure 6 Evolution and product flow in μPIM.

1.16.3 PIM Process

Remarkable advancements have been achieved over the years as researchers have focused on process development, tooling, and product quality improvement of PIM. An illustration of the process and product flow during various processing steps of the μPIM process is shown in Figure 6.

As illustrated in Figure 6, PIM is developed from process integration of plastic injection molding and powder metallurgy. As stated, PIM covers injection molding of both CIM and MIM. In addition, MIM is further divided into convectional MIM and μMIM processes. Regardless of the scale (macro, meso, micro, nano) or material (ceramic or metal powder) involved, PIM undergoes four processing steps: feedstock preparation (mixing

of powder-binder constituents), injection molding (mold cavity filling by melt), debinding, and sintering.

1.16.3.1 Feedstock Preparation

Manufacture of parts and components by PIM began from feedstock preparation, which involves the blending of the micrometal or ceramic powder with the polymeric binder in an appropriate composition. The percentage volume fraction of the binder depends on material properties of the constituents and those of the metal or ceramic powder. Investigation of μPIM began with commercial available feedstocks that are used for conventional PIM. However, the use of convectional powder results in many cases of part defects and poor shape retention of the microcomponents.[31] Therefore, there is a need for modified feedstock systems that are suitable for μPIM. This geared researchers' attention toward material type, powder size, binder composition, mixing ratios, and feedstock characterization, which are among many factors considered during investigations.[2]

However, reliable feedstocks are now available. Those who are new to PIM production will have to make a decision regarding whether to purchase a ready-made feedstock from a specialized supplier or to develop and manufacture in-house. There is no right or wrong decision here, because both choices have advantages and disadvantages. In the past, for some pioneers of MIM parts producers, there was no choice. No feedstock suppliers existed in the early days of MIM. Therefore, these companies and individuals have acquired a license or tried to develop binder systems for use at that time. Presently, there are various 'ready to mold' feedstock suppliers who offer a diverse range of off-the-shelf feedstock as well as that customized to specifications as demanded by the user. One of the main secrets of successful MIM fabrication is to maintain absolute batch-to-batch consistency in feedstock production. If this is not achieved, then the production process is prone to product defects during molding, as well as distortion and other voids.

Then, for those who wish to manufacture feedstock in-house, there is a need for in-depth understanding of binder systems development. In addition, know-how is required regarding the use of mixing tools such as the screw extruder, Z-blade, and double planetary mixers. These are various mixing mechanisms used for blending and compounding powders/binder constituents to produce injection molding feedstock. Some fundamental parameters of feedstock preparation are mixing temperature, mixing time, rotor geometry, rotational speed, and powder loading, respectively. For feedstock mixing operations, the work energy (E_t) supplied to the system by the rotors is the product of force by the distance (d) covered and expressed as:

$$E_t = F.d \quad [9]$$

$$E_t = 2\pi rN \int_{t1}^{t2} \left(\frac{M(t)}{r}\right) \mathrm{d}t \quad [10]$$

where N is angular speed expressed in rpm, r is the average blade radius, t is time, and $M(t)$ is the torque and expressed as:

$$M(t) = F.r$$
$$\mathrm{TTQ} = r \int_{t1}^{t2} \left(\frac{M(t)}{r}\right) \mathrm{d}t \quad [11]$$

$$\therefore E_t = 2.\pi.N.\mathrm{TTQ} \quad [12]$$

The work energy is expressed as a function of totalized torque (TTQ) in eqn [12]. Specific processing energy (E_{sp}) in the mixing chamber as a function of E_t is expressed as:

$$E_{sp} = \frac{E_t}{m_{\mathrm{feedstock}}} \quad [13]$$

where m_{feed} represents the mass of the feedstock within the mixing chamber. The specific energy dissipated by friction can be assessed by considering the overheating of the feedstock together with the specific heat of the feedstock ($C_{\mathrm{feedstock}}$)

$$E_{\mathrm{friction}} = C_{\mathrm{feedstock}} \Delta T_{\mathrm{oh}} \quad [14]$$

where ΔT_{oh}, is the change in temperature of overheating.

Typically, an overview of feedstock preparation involves characterization of the metal powder, binder, feedstock formulation, and characterization.

1.16.3.1.1 Metal powder

The process of MIM is possible with any metal that can be produced in a suitable powder form. The technology is successful for plain and low-alloy steels, stainless steels, high-speed steels, copper-based alloys, nickel-based and cobalt-based superalloys, titanium, intermetallics, magnetic alloys, refractory metals, and hard metals (cemented carbides).[32] But processing some metals such as aluminum and magnesium is challenging due to the occurrence of adherent oxide film, although such difficulties can be overcome. The production techniques and attributes of MIM powders are presented in Table 4.[32–33]

In addition, mechanical crushing/grounding is sometimes used when minor powder additions are required for elemental

Table 4 Production techniques and attributes of metal injection molding powders

Production techniques	*Suitable metals or alloys*	*Particle size (μm)*	*Shape*	*Relative cost*
Gas atomization	Metals, alloys	5–45	Spherical	High
Water atomization	Metals, alloys	5–45	Semi-spherical/irregular	Moderate
Thermal decomposition	Metals	0.2–20	Spherical, spiky	Moderate
Chemical reduction	Metals	0.1–10	Angular, spherical	Moderate

Source: Modified from Enneti, R. K.; Onbattuvelli, V. P.; Atre, S. V. 4 – Powder Binder Formulation and Compound Manufacture. In Metal Injection Molding (Mim). In *Handbook of Metal Injection Molding*; Heaney, D. F., Ed.; Woodhead Publishing, 2012; pp. 64–92; From EPMA. *Metal Injection Moulding – A Manufacturing Process For Precision Engineering Components*, 3rd ed.; European Powder Metallurgy Association (EPMA), 2013.

powder blends to produce a given alloy composite. A typical metal powder is characterized by size, size distribution, and shape.[33] Powder characteristics and various test standard are presented in Table 5.

Particle size distribution (PSD) is an important factor considered in PIM processes. Typical PSD for coarse powder (INV1) and fine powder (INV2) feedstock is shown in Figure 7. Typical PSD of a metal powder is characterized by d_{10}, d_{50}, and d_{90}. In simple terms, $d_{10} \approx 2\ \mu m$, $d_{50} \approx 5\ \mu m$, and $d_{90} \approx 10\ \mu m$, respectively. The d_{10} is a size where 10% of the particles are less than this size. Likewise, the d_{50} is a size where 50% of the particles are less than this size. Meanwhile, metal powder suppliers, most of the time, sell their products as d_{90} sizes; a d_{90} of 22 μm has 90% of the particles less than 22 μm. However, one must be careful because some powders are sold as d_{80} sizes, which means that 80% of the particles are less than the actual size. It is then important to note the PSD of the powders before use, because powder behaves differently during compounding, molding, and sintering. For instance, a smaller d_{10} will be finer and subsequently sinter better, but will load poorly into a binder system, whereas a large d_{90} will have more coarse particles and sinter poorly. In addition, the spherical powders are preferred for high packing density and flow characteristics of MIM feedstock; however, some advantages in shape retention have been seen with slightly irregularly shaped particles.[34]

Typically, μMIM is performed using micrometal powders of a medium size for various shapes, as presented in Table 4. As a general rule, the powder particle sizes should amount to no more than one-tenth or, preferably, one-twentieth of the size of the smallest detail of the cavity. The d_{50} values of the steels are typically in the range of 1.5–4.5 μm. Fractions up to 10 μm or more have been used successfully. For instance, PSD and S_W (width of the PSD) of INVAR 36 feedstock are presented in Table 6.[35]

1.16.3.1.2 Binder

The binder is a major constituent of PIM feedstock preparation. Its formulation consists of at least two components that are referred to a major component (e.g., wax) and a secondary component that is usually a high-molecular-weight polymer. In general, binder systems used in MIM are classified into four main categories: wax-based binder; water-soluble binder; polyoxymethylene-based binder; and aromatics-based binder system.[36]

The wax-based binder comprises the thermoplastic or thermoset-based polymers, and these binder systems have been used successfully for titanium, steel, tungsten, and ceramic powder. The wax component in wax-based binder systems is used to wet the metallic powder particles, whereas the polymeric component provides sufficient green strength. Typically, waxes such as paraffin wax (PW), beeswax (BW), carnauba wax (CW), and several wax-like short oligomers or low-molecular-weight polymers are mostly used. The popular backbone polymers used in wax-based binder systems are polyethylene (PE), polypropylene (PP), ethylene vinyl acetate (EVA), and high-molecular-weight polymethyl methacrylate (PMMA). Table 7 presents the typical composition of a PW-based binder system.[36]

Table 5 Powder characteristics and test standard

Powder characteristics	*Test standard*
Pycnometer density (PD)	MPIF 63, ASTM D 2638, ASTM D 4892
Apparent density	MPIF 28 and 48, ASTM B 417 and B 703, ISO 3923–1 and 3953
Tap density	MPIF 46, ASTM B 527, ISO 3953
Particle size distribution	ASTM B 822–10, ISO 13320–1

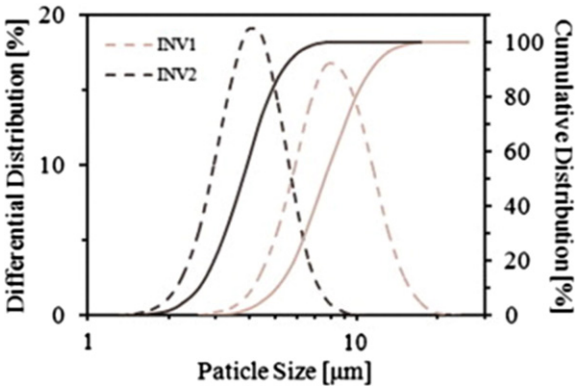

Figure 7 Typical particle size distribution for INV1 and INV2 feedstock. Hidalgo, J.; Jiménez-Morales, A.; Barriere, T.; Gelin, J. C.; Torralba, J. M. Capillary Rheology Studies of Invar 36 Feedstocks for Powder Injection Moulding. *Powder Technol.* **2015**, *273*, 1–7.

Table 6 Particle size distribution of INVAR 36 alloy powders

Powder	*Particle size (μm)*					S_w
	d_{10}	d_{50}	d_{60}	d_{90}	$d_{60}/(d_{60}+d_{60})$	
INV1	5.05	7.69	8.33	11.44	0.214	7.21
INV2	2.60	3.81	4.09	5.29	0.413	8.30

Source: Hidalgo, J.; Jiménez-Morales, A.; Barriere, T.; Gelin, J. C.; Torralba, J. M. Capillary Rheology Studies of Invar 36 Feedstocks for Powder Injection Moulding. *Powder Technol.* **2015**, *273*, 1–7.

Table 7 Typical composition of PW-based binder system

Wax component	*Polymeric component*	*Surfactant*
PW + CW	PP + EVA	DOP
PW	PE + PMMA	SA
PW	PEG + PE	SA
PW	PE	SA
PW + CW	Atactic PP	SA
PW	PP + EVA + PE	SA
PW	PP + PE + PEG	SA

Abbreviations: CW, Carnauba wax; DOP, Dioctyl phthalate; EVA, Ethylene vinyl acetate; PEG, Polyethylene glycol; PMMA, Polymethylmethacrylate; PP, Polypropylene; PW, Paraffin wax; SA, Stearic acid.

Source: Modified from Wen, G. A.; Cao, P.; Gabbitas, B.; Zhang, D.; Edmonds, N. Development and Design of Binder Systems for Titanium Metal Injection Molding: An Overview. *Metallurgical and Materials Transactions A – Physical Metallurgy and Materials Science* **2013**, *44A* (3), 1530–1547.

Wax-based binders have been widely used in the PIM. However, the solvent debinding process of extracting wax from the green parts used solvents such as heptanes and hexanes. These solvents, when disposed after use, are toxic to the environment. This problem then necessitates the development of new, alternative, environmentally friendly binders that can be extracted by nontoxic solvents such as ethanol and water. In 1976, the first water-soluble binder, methylcellulose or polyvinyl alcohol (PVOH), was disclosed.

According to Wen *et al.*,[36] water-based binders are classified into two categories based on the interaction of the binder component and water: gelation-based and nongelation based. The nongelation-based binders do not need water for the feedstock formulation, but water is used for the binder extraction during the debinding process. Synthetic polymeric components of the water-based binder include polyethylene glycol, polyethylene oxide, and/or PVOHs and are commonly used. After injection of the feedstock, the green part is soaked in the water to extract the nongelation-based component. However, the gelation-based binders usually include solvents when formulating the feedstock; water is the most commonly used, but others like glycerol are also possible. The formulation process of the gelation-based binder begins when the binder interacts with water molecules to form gel using the binder composite. This is achieved either before or during feedstock formulation; sometimes, feedstock compounding and injection molding are combined in one step. The green part is then dried to remove the water molecules. Subsequently, the remaining portions of the binder polymers and other additives are removed by thermal debinding. Thermal debinding and sintering are sometimes combined into one single step for gelation-based binder feedstock.

1.16.3.1.3 Feedstock formulation and characterization

Selection and formulation of binder constituents are critical in PIM. The success of a defect-free molded part is achieved by appropriate formulation of the binder system.[37–40] It is important to note that the powder loading of the feedstock is expressed in terms of the volumetric or weight percentage. A typical volumetric percentage proportion of the powder ranges between 35 and 50 vol.%.[41] **Table 8** summarizes some selected metal powders, binder constituents, and optimal powder loading of MIM feedstock from the literature.

In addition, attributes of feedstock in PIM are its powder characteristic, binder composition, powder-to-binder ratio, and mixing method, respectively. Therefore, a study of the effect of processing conditions and feedstock characteristics is required for producing quality finished parts.[53–59] Equation [15] is used for estimating the appropriate volumetric fraction of the feedstock composite

$$\phi_p = \frac{\frac{X_p}{\rho_p}}{\frac{X_p}{\rho_p}+\frac{X_b}{\rho_b}}, \quad \phi_b = \frac{\frac{X_b}{\rho_b}}{\frac{X_p}{\rho_p}+\frac{X_b}{\rho_b}} \qquad [15]$$

Alternatively, the mass fraction can be calculated using eqn [16] as:

$$X_p = \frac{\phi_p\rho_p}{\phi_p\rho_p+\phi_b\rho_b}, \quad X_b = \frac{\phi_b\rho_b}{\phi_p\rho_p+\phi_b\rho_b} \qquad [16]$$

The subscripts p and b denote metal powder and binder. ϕ and X represent the volume and mass fraction of the composite. However, for the feedstock formulation design, the binder is considered a vehicle of transportation. Therefore, it is important to note that a good binder must fulfill the following conditions: good flow characteristics; comparatively low cost; good interactions with metal powders; enables easy debinding; and environmentally safe and/or easily disposable after debinding.[37,60–62]

Typical feedstock in MIM is composed of a fine metal powder and binder system. The binder is designed to provide flowability characteristics during the injection molding process and structural rigidity of the green part during debinding and sintering steps of MIM. A number of binder systems have been designed, including wax–polymer, water-soluble, catalytic debindable, and water–gel-based systems. These binder systems are solid at room temperature, and they then go through a few melting transitions during processing. This occurs for each constituent component of the binder until the entire system is molten, with the exception of the water–gel-based binder systems as described previously. Processing is performed at temperatures above the final melt temperature of the binder system but well below the decomposition temperature.[63] In addition, feedstock behavior is predicted through rheological properties analysis.

Rheology, burnout, and enthalpy of fusion of the feedstock are measured using techniques such as capillary rheometry,[35,64] thermogravimetric analysis (TGA), and differential scanning calorimetry (DSC).[60] In addition, the homogeneity of the feedstock is performed to determine the powder–binder composition and dispersion of powder within the feedstock pellets. **Table 9** presents test standards, equipment, and feedstock property.

The capillary and torque rheometer are used to measure the rheological characteristics of the feedstocks. The technique of capillary rheometer is based on measuring the pressure drop and flow rate as the feedstock is forced through a small gap. Likewise, the torque rheometer measures the torque required for mixing the feedstock as a function of time. The capillary rheometer technique is widely used and mostly preferred because the flow of the feedstock through the capillary rheometer is similar to the melt filling the mold cavity during the IM process. Therefore, the determination of the feedstock material properties, powder loading, activation energy, moldability index, and critical powder volume concentration (CPVC) are among the quantities investigated in PIM. Accurate measurement and determination of material properties (such as rheological, thermal, and mechanical properties) are expensive and time-consuming.[65] However, quite a few empirical models were developed to predict these properties with high accuracy for various feedstock (powder–polymer mixture). Based on the general rule of mixtures, the relationship for estimating these properties are presented as:

(1) Density

$$\frac{1}{\rho_f} = \frac{X_p}{\rho_p}+\frac{X_b}{\rho_b} \qquad [17]$$

Table 8 Composite and formulation of some selected metal injection molding feedstock

Metal powder	*Binder constituent*	*Powder loading*	*Reference*
316L Stainless steel	73% Polyethylene glycol, 25% polymethyl methacrylate, and 2% SA	68% vol.	Rajabi *et al.*[42]
316L Stainless steel	41.3 wt% Starch, 23.3 wt% glycerol, 28.5 wt% linear low-density polyethylene, 1.9 wt.% citric acid, 5 wt% SA	57% vol.	Abolhasani and Muhamad[43]
316L Stainless steel	45 wt% Low-density polyethylene, 55 wt% PW, 5 wt% SA	–	Setasuwon *et al.*[44]
316L Stainless steel	45 wt% Low-density polyethylene, 45 wt% PW, 10 wt% palm oil, and 5% wt% SA	–	Setasuwon *et al.*[44]
316L Stainless steel	30% PW, 10% CW, 10% BW, 45% ethylene vinyl acetate, 5% SA		Supriadi *et al.*[45]
316L Stainless steel	30% PW, 10% CW, 10% BW, 45% polypropylene, 5% SA		Supriadi *et al.*[45]
316L Stainless steel	25% PW, 20% CW, 20% BW, 25% ethylene vinyl acetate, 5% polypropylene, 5% SA		Supriadi *et al.*[45]
316L Stainless steel	73 wt% Polyethylene glycol, 25 wt% polymethyl methacrylate, and 2 wt% SA	62% vol.	Rajabi *et al.*[42]
316L Stainless steel	85% PW, 15% ethylene vinyl acetate	–	Shimizu *et al.*[46]
316L Stainless steel	65% PW, 35% ethylene vinyl acetate		Shimizu *et al.*[46]
316L Stainless steel	70% PW, 25% polyethylene, 5% SA		Shimizu *et al.*[46]
316L Stainless steel	75% PW, 20% polyethylene, 5% ethylene vinyl acetate		Shimizu *et al.*[46]
316L Stainless steel	75% PW, 15% polyethylene, 10% ethylene vinyl acetate		Shimizu *et al.*[46]
17–4PH Stainless steel	64% PW, 16% MW, 15% EVA, and 5% HDPE	60% vol.	Li *et al.*[47]
17–4PH Stainless steel	63% PW, 16% MW, 15% EVA, 5% HDPE, and 1% SA	60% vol.	Li *et al.*[47]
17–4PH Stainless steel	59% PW, 16% MW, 15% EVA, 5% high-HDPE, and 5% SA	60% vol.	Li *et al.*[47]
17–4PH Stainless steel	55% PW, 16% MW, 15% EVA, 5% high-HDPE, and 9% SA	60% vol.	Li *et al.*[47]
Zirconia-toughened alumina	50% HDPE, 46% PW, and 4% SA	57% vol.	Ani *et al.*[48]
HS12–1–5–5 high-speed steel	50% HDPE, 50% PW	68% vol.	Dobrzański *et al.*[49]
Copper	65% PW, 30% polyethylene, 5% SA	95% wt.	Moballegh *et al.*[50]
Iron–nickel	79% PW, 20% ethylene vinyl acetate, 1% SA	58% vol.	Huang *et al.*[51]
Iron–nickel	79% PW, 20% HDPE, 1% SA	58% vol.	Huang *et al.*[51]
Iron–nickel	79% PW, 10% HDPE, 10% ethylene vinyl acetate, 1% SA	58% vol.	Huang *et al.*[51]
Iron–nickel	55% PW, 25% polypropylene, 15% carnauba, 5% SA	55% vol.	Lin[52]
Aluminum	35% Polypropylene, 60% PW, and 5% SA	62% vol.	Abdoos *et al.*[40]

Abbreviations: BW, Beeswax; CW, Carnauba wax; EVA, Ethylene-vinyl acetate copolymer; HDPE, High- density polyethylene; MW, Microcrystal paraffin wax; PW, Paraffin wax; SA, Stearic acid.

where ρ is the density, X is the mass fraction, and the subscripts f, b, and p stand for the composite, binder, and powder, respectively.

(2) Viscosity

$$\eta_c = \frac{\eta_p}{\left[1 - \left(\phi_p/\phi_{\max}\right)\right]^2} \quad [18]$$

where η is the viscosity and ϕ is the volume fraction. The subscripts c and p stand for composite and powder, respectively.

(3) Specific heat

$$C_{pc} = \left[C_{pb}X_b + C_{pp}X_p\right] \quad [19]$$

where C_p is the specific heat, X is the mass fraction, and the subscripts c, b, and p stand for the composite, binder, and powder, respectively.

(4) Specific volume

$$V_c = X_p V_p + V_b\left(1 - X_p\right) \quad [20]$$

where V is the specific volume, X is the mass fraction, and the subscripts c, p, and b refer to the composite, powder, and binder, respectively.

(5) Thermal conductivity

$$\lambda_c = \lambda_b\phi_b + \lambda_p\phi_p \quad [21]$$

where λ is the thermal conductivity and ϕ is the volume fraction. The subscripts c, p, and b denote composite, powder, and binder, respectively.

(6) Coefficient of thermal expansion

$$\alpha_c = X_p\alpha_p + \alpha_b\left(1 - X_p\right) \quad [22]$$

where α is the thermal expansion coefficient and X is the mass fraction. The subscripts c, p, and b denote composite, powder, and binder, respectively.

(7) Elastic and shear modulus

$$E_c = E_p X_p + E_b(1 - X_b) \quad [23]$$

where X is the mass fraction and E is the elastic or shear modulus. The subscripts c, p, and b represent composite, powder, and binder, respectively.

(8) Moldability index

$$\alpha_{stv} = \frac{1}{\eta_0} \frac{\left|\frac{\partial \log \eta}{\partial \log \dot{\gamma}}\right|}{\frac{\partial \log \eta}{\partial (1/T)}} = \frac{1}{\eta_0} \frac{1-n}{E/R} \quad [24]$$

where α_{stv} is the moldability index and the subscripts s, t, and v represent the effect of shear, temperature, and viscosity sensitivity, respectively. η_0 is the reference viscosity at a specified temperature and $\dot{\gamma}$ is shear rate.

(9) Critical powder volume concentration

$$\text{CPVC} = \frac{V_p}{(V_p + V_L)} \times 100 \quad [25]$$

Table 9 Equipment, test standards, and feedstock property

Test standard	*Equipment*	*Feedstock property*
ASTM D3835	Capillary rheometer	Rheology (viscosity, shear rate, temperature)
ASTM E1269	Differential scanning calorimeter (DSC)	Specific heat
ASTM D7426	DSC	Solidification
ASTM D3418	DSC	Melting
ASTM E1131	Thermogravimetric analysis	Burnout
ASTM D638	Universal testing machine	Elastic modulus and Poisson's ratio
ASTM E831	Thermomechanical analyzer	Coefficient of thermal expansion
ASTM D792	High-pressure dilatometer	Pressure–volume–temperature
ASTM D5930	Line source method	Thermal conductivity

where V_p is the powder volume and V_L is the oil volume at the CPVC point, respectively.

1.16.3.2 Injection Molding Process

Microinjection molding includes both PIM and plastic injection molding at microscale. Basically, during this processing step, the feedstock is fed into the IMM, which uses a screw-type plunger or ram to force melt into the mold cavity. However, the μIM process is more than just scaling down of the conventional injection molding; it requires a thorough rethinking of the entire process.[29,66,67] Therefore, μIM requires special attention to the processing conditions using basic principles of operation of the convectional IM.

1.16.3.2.1 Principles of microinjection molding

As the feedstock is fed through the hopper, the clamping mechanism of the IMM closes the mold. Then, the feedstock begins to melt and is usually maintained at a constant temperature. Afterward, the melt is injected into the closed mold cavity by a ram or a screw-plunger of the injection unit acting as a piston. The melt is then cooled to take the shape of the mold cavity. During this processing cycle, the part is held under pressure by the injection unit to compensate for the thermal shrinkage. After solidification of the molded part, the mold is opened by the machine actuator of the clamping unit and the final part is ejected.[68] These operations are continuously repeated in a sequential order called the injection molding cycle.

1.16.3.2.2 Injection molding cycle

In a typical commercial IMM, injection of melt is characterized by a sequence of operations referred to as the molding cycle. The operation basically begins by closing the mold, injecting the melt into the mold cavity, holding pressure, refilling and cooling, and opening the mold to eject the part; the process is repeated continuously, as illustrated in Figure 8.[69]

As shown in Figure 8, the injection molding cycle consists of the following phases: injection, pack, hold, and cooling, respectively. In addition, these distinct phases or operations are associated with process parameters, which are categorized into four broad headings: pressure, speed, time, and temperature. Hence, it is important to note that monitoring and

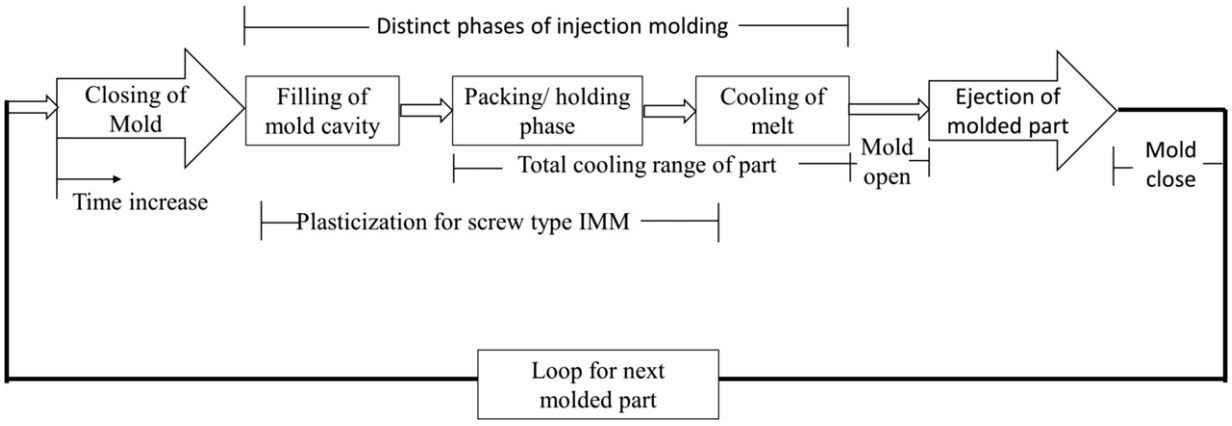

Figure 8 Injection molding cycle.

controlling of these parameters enhance part quality, but some are more critical.

1.16.3.2.3 Critical factors influencing part quality in IM

The choices of IMM, feedstock material selection, process condition, mold, and part design are critical factors that influence molded part quality in injection molding.[70] According to Surace *et al.*,[71] researchers investigated the optimum processing conditions for microfabrication of various parts. The following process parameters were found to affect part quality in μIM: mold temperature, melt temperature, injection speed, injection pressure, holding time, holding pressure, and cooling time. Therefore, application of optimization techniques to μIM processes will enhance molded part quality and lead to less scrap, efficient cycle times, and improved productivity.

1.16.3.3 Debinding Process

This is the process of binder removal. It is described as the most complex, difficult, expensive, and time-consuming stage, and it depends on processing conditions. In line with the formulation of the binder constituent, the minor binder components (such as plasticizers, surfactants, and lubricants) are usually removed first and the backbone binder component is removed last. In practice the debinding techniques adopted are solvent debinding,[72–73] thermal debinding,[74–75] catalytic debinding,[76] and wicking debinding,[77] respectively.

A multi-step debinding technique is now practiced, whereby the green part is processed via solvent medium (such as hexane and heptane) and then followed by thermal debinding. The multistep technique is preferred as a result of defects associated with direct thermal debinding such as cracking, slumping, porosity, and blistering.[78,79] Combining solvent and thermal debinding techniques reduces processing time; the parameters are presented in **Table 10**.

The fundamental principles of the solvent and thermal debinding techniques are discussed next.

1.16.3.3.1 Solvent debinding

This is a technique that removes the binder constituent of the feedstock using solvent. The green part is immersed in the solvent (such as water, hexane, heptain, acetone, ethanol, and other alcohols). At specified temperatures, binder constituent is dissolved in liquid at low temperatures and a network of interconnected porosity is formed in the part while being immersed in the solvent. However, most of available solvents used are dangerous to the environment if necessary precautions and measures are not observed. Meanwhile, water is identified as a safe solvent that is environmentally friendly. Solvent debinding requires a longer time to remove binder constituent relative to other techniques, such as catalytic and thermal debinding processes. Cost and environmental challenges are much lower, especially when water is used.

Table 10 Some process parameters of solvent and thermal debinding technique

Debinding technique	*Process parameters*
Thermal	Heating rate, holding temperature, holding time, cooling rate
Solvent	Immersion time, immersion temperature, dissolving medium

1.16.3.3.2 Thermal debinding

The polymeric constituent of the binder system can be eliminated by heating the green part to temperatures that cause the main polymers to decompose or degrade. The temperature could be up to 800 °C, but it strongly depends on the binder system. Meanwhile, the thermal binder burnout requires times longer than for catalytic debinding. To reduce the processing time, a combination of solvent and thermal debinding is usually adopted. Herranz *et al.*[80] used a PE-based binder system and demonstrated the successful application of the double-cycle debinding process involving solvent (heptane solvent) debinding and thermal debinding.

The use of a thermal debinding technique is widely practiced due to its high efficiency in binder burnout, but the occurrence of part defects has limited the practice as a standalone method. Therefore, the double-stage method, which involves solvent and thermal energy, is mostly practiced. The process is simple and similar to the sintering process. Therefore, it is widely accepted and used. Typically, the burnout of the polymeric constituent from the green part involves chemical and physical mechanisms.

The chemical mechanisms occur because of thermal degradation of polymers into volatile species, called pyrolysis. The physical mechanisms involve diffusion of the volatile species to the surface and changes in the polymer distribution within the green body. Depending on the material properties, such as thermal conductivity, porosity, pore size, and related features, it is possible for mass diffusion or thermal diffusion to be controlling steps. As a further complication, component heating depends on heat transfer and the reaction enthalpies associated with pyrolysis events, leading to thermal–kinetic effects that couple to the chemical–physical aspects.

1.16.3.3.3 Other debinding techniques

Apart from the solvent and thermal debinding methods, other techniques such as catalytic debinding and wicking debinding are practiced. The uses of other techniques, other solvents, and thermal debinding arise as a result of the requirements of the binder formulation or composite such as polyacetal. The polyacetal binder systems require debinding in a gaseous acid environment (usually highly concentrated nitric or oxalic acid) at a temperature of approximately 120 °C (a temperature slightly lower than that for softening the binder system). The nitric or oxalic acid used served as a catalyzer in the degradation of the polyacetal constituent of the binder system.

1.16.3.3.4 Development of master decomposition curve

The design and optimization of the debinding process are enhanced through effective investigation and development of the master decomposition curve (MDC) for the polymeric binder component of the feedstock. This is an essential tool used for the prediction of part behavior at the debinding step, a process that is viewed to be a challenging task for PIM. This is due to the fact that several researchers have reported that the process of binder removal from the green part is expensive and

time-consuming, and is sometimes viewed as a limitation for PIM processing. According to Aggarwal *et al.*,[81] the feedstock of PIM consists of multiple components that can be categorized into two groups according to their molecular weight as:

- Low-molecular-weight polymers, such as solvents and plasticizers, that can either be evaporated or are decomposed at low temperatures.
- High-molecular-weight polymers, such as polymers possessing higher thermal stability, that are pyrolyzed at relatively high temperatures.

Therefore, the need for the kinetic investigation of the binder components of the molded part during debinding is paramount and monitored through weight loss. The TGA and differential thermal analysis are used extensively for the determination of weight loss of the binder component as a function of time and temperature. **Figure 9** illustrates a typical TGA plot of the binder components at various rates in an argon atmosphere.

The concept of the master sintering curve (MSC), developed by Su and Johnson,[82] successfully extended to include binder behavior during solvent extraction and wicking process of debinding, respectively.[72] The MDC was developed for single-step and multistep burnout of the polymeric binder and is presented in the next section.

1.16.3.3.4.1 Single-step burnout process

Depolymerization of polymeric binders can be described by first-order reaction kinetics. The remaining weight fraction of a polymer, α, is expressed as[83,84]:

$$\frac{d\alpha}{dt} = -K\alpha \qquad [26]$$

where t is the time and K is the rate constant for degradation and relate to the Arrhenius eqn [27]:

$$K = K_0 \exp\left(\frac{-E}{RT}\right) \qquad [27]$$

where K_o is the specific rate constant, E is the apparent activation energy for thermal degradation, R is the gas constant, and T is the absolute temperature. Combining eqns [26] and [27] provides the following:

$$-\int_1^{\alpha} \frac{d\alpha}{\alpha} = -\ln \alpha \qquad [28]$$

$$-\ln \alpha = \int_0^t K_0 \exp\left[-\frac{E}{RT}\right] dt = K_0\Theta \qquad [29]$$

Where the decomposition (ψ) is expressed as:

$$\Theta(t, T; Q) = \int_0^t K_0 \exp\left[-\frac{E}{RT}\right] dt \qquad [30]$$

$$\alpha(\Theta; K_0) = \exp[-K_0\Theta] \qquad [31]$$

Equation [30] defines the MDC, where the decomposition curves for a given polymer with any decomposition cycle uses the concept of work of decomposition, Θ.

In addition, Enneti *et al.*[72] proposed a modification to the MSC by incorporation of the shape factor. The modified MSC is capable of estimating activation energy without further dependency on solvent extraction rate to the square of the length of the part as previously practiced. The fundamental MSC model is expressed as eqn [31], whereas the modified MSC for the prediction of activation energy during solvent extraction and wicking process is given by eqn [32].[72]

$$\Phi(\rho) = \theta(t, T) = \int_0^t \frac{1}{T} \exp\left(\frac{-E}{RT}\right) dt \qquad [32]$$

$$\Phi(\rho) = \theta(t, T) = \left(\tfrac{1}{\psi^2}\right) \int_0^t \frac{1}{T} \exp\left(\frac{-E}{RT}\right) dt \qquad [33]$$

where $\Phi(\rho)$ is the densification, ψ is the shape factor, t is the time, T is the absolute temperature, E is the apparent activation energy, and R is the universal gas constant.

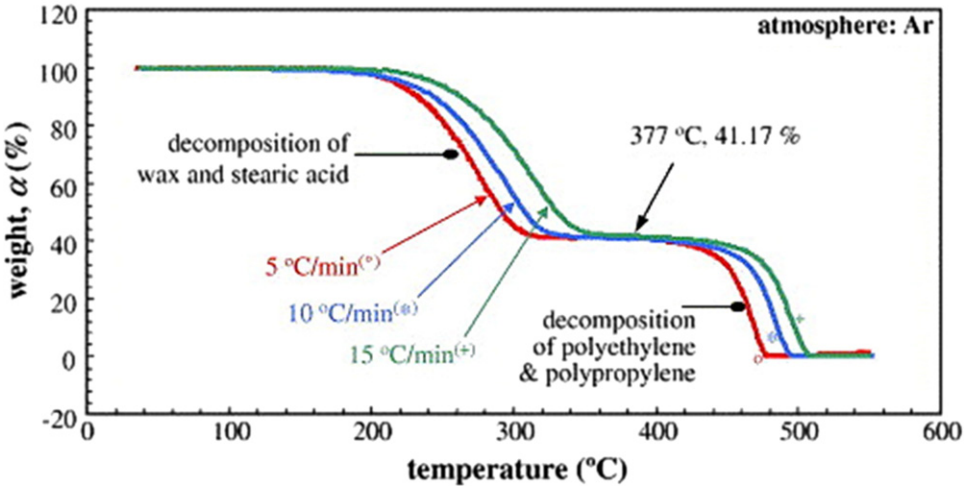

Figure 9 A typical thermogravimetric analysis plot of binder components at various rates. Aggarwal, G.; Smid, I.; Park, S. J.; German, R. M. Development of Niobium Powder Injection Molding. Part II: Debinding and Sintering. *Int. J. Refract. Metals Hard Mater.* **2007**, *35*, 226–236.

1.16.3.3.4.2 Evaluation of apparent activation energy

To evaluate the decomposition (Θ) from eqn [30], the apparent activation energy (E) needs to be determined. The activation energy for polymeric binder decomposition can be determined from TGA data using the Kissinger method. The temperature (T_{max}) at which the maximum rate of weight loss occurs at various heating rates is used for the determination as follows:

$$\frac{d}{dt}\left(-\frac{d\alpha}{dt}\right)=0 \text{ and } T=T_{max} \quad [34]$$

considering constant heating rate (r) and then

$$\frac{dT}{dt}=r \quad [35]$$

$$\frac{rE}{RT_{max}^2}=K_0 \exp\left(\frac{-E}{RT_{max}}\right) \text{ at } T=T_{max} \quad [36]$$

Equation [36] is simplified in linear form and expressed as:

$$\ln\left[\frac{r}{T_{max}^2}\right]=E\left(-\frac{1}{RT_{max}}\right)-\ln\left[\frac{E}{K_0R}\right] \text{ at } T=T_{max} \quad [37]$$

The apparent activation energy E of the reaction represents the slope from a plot of $\ln\left(\frac{r}{T_{max}^2}\right)$ and $\left(-\frac{1}{RT_{max}}\right)$, which are determined from the TGA experiments with several constant heating rates.

However, Aggarwal *et al.*[84] proposed a statistical approach for the determination of the apparent activation energy based on the MDC concept. The idea is to minimize the mean residual (MR) while varying the activation energy. MR is mathematically defined as follows:

$$MR=\sqrt{\int_t^0\left[\frac{\sum_{i=1}^{N}\left(\frac{\Theta_i}{\Theta_{avg}-1}\right)^2}{N}\right]d\alpha} \quad [38]$$

where N is the number of TGA experiments, i is the running index for the TGA experiment label, Θ_i is the work of decomposition calculated from TGA experiments with the label of i, and Θ_{avg} is the average work of decomposition calculated from all TGA experiments, respectively. This alternative method is simple because it does not attach any condition to the TGA experiments. The two methods are derived from the same fundamental equations.

1.16.3.3.4.3 Multistep burnout process

Typical TGA curves of polymer degradation follow a single sigmoidal path. However, multicomponent binder systems may have two or more sigmoids due to the different molecular weights, bonding groups, and degradation paths for each polymer constituents. Then, each sigmoid describes a rate-controlling step whose activation energy differs from those of other controlling steps. It is then important to remember that powder–binder systems in PIM often consist of several components. Typically, the binder components can be categorized into two groups based on molecular weight of the constituents: high-molecular-weight (HMW) and low-molecular-weight (LMW). The LMW ones are additives such as solvents and plasticizers, which either evaporate or decompose at low temperatures. Whereas the HMW polymers are characterized as possessing higher thermal stability and decomposing at high temperatures relative to the LMW. Therefore, the difference in molecular weight of the PIM binder system is responsible for the TGA curve with multiple sigmoids. Superposition of several sigmoids may be observed when the constituents have similar activation energy. Sigmoids typically represent a distinct reaction step with sufficiently different activation energy. A sigmoid is described by three kinetic parameters in reference to the Arrhenius equation. The frequency factor, activation energy, and reaction order are used for distinguishing each sigmoid that represents each powder. However, some powders may have catalytic effects on the pyrolysis rate; however, the shape of the pyrolysis curve with powders is similar to that without powders.

Therefore, the mathematical form of polymer pyrolysis can still be applied. Two polymers of the binder system used in this study are decomposed during the thermal debinding process:

$$\alpha=\omega\alpha_1+(1-\omega)\alpha_2 \quad [39]$$

where α is the mass ratio of the initial masses of two polymers, α_1 is the ratio of mass to initial mass of the low-molecular-weight polymer, α_2 is the ratio of mass to the initial mass of the high-molecular-weight polymer, and ω is the ratio of the initial mass of the low-molecular-weight polymer to the initial mass of the two polymers.

The mathematical form that is generally applied to the TGA curve of a polymer is modified to describe the TGA curve of organic pyrolysis with powders. In the present analysis, we assume that the kinetics are solely controlled by the temperature:

$$-\frac{1}{k_0\beta^n}d\alpha=\exp\left[-\frac{E}{RT}\left(\frac{1}{T}-\frac{1}{T_t}\right)\right]dt$$

$$\text{if } T\geq T_t(\text{or } \alpha\geq\omega),\ \alpha=\omega\alpha_1+(1-\omega),$$

$$\beta=\frac{\alpha+(\omega-1)}{\omega},\ n=n_1\ K_0=K_{01},\ E=E_1$$

$$\text{if } T>T_t(\text{or } \alpha<\omega),\ \alpha=(1-\omega)\alpha_2,$$

$$\beta=\frac{\alpha}{(1-\omega)},\ n=n_2\ K_0=K_{02},\ E=E_2 \quad [40]$$

where T_t is the transition temperature between the first and second sigmoids, and subscripts 1 and 2 that appear along with a, E, and K_0 represent the low- and high-temperature degradation, respectively. In addition, it is possible to evaluate a decomposition kinetic curve with more than two sigmoids using the concept described. Meanwhile, the Kissinger method is applied to estimate the activation energy, as described in Section 1.16.3.3.4.2.

Splitting eqn [40] and integrating each side separately is expressed as the left side of eqn [40] as a function of the mass ratio α and material properties K_0, yielding:

$$\Phi(\alpha; k_0) = \int_1^{\alpha} \frac{1}{K_0 \beta^n} d\alpha \qquad [41]$$

Likewise, integrating the right side of eqn [40] is expressed as a function that depends on t, T, E, and T_t:

$$\Theta(t, T; E, T_t) = \int_0^t \exp\left[-\frac{E}{R}\left(\frac{1}{T} - \frac{1}{T_t}\right)\right] dt \qquad [42]$$

where $\Phi(\alpha)$ is considered a characteristic that quantifies the effect of binder components on the decomposition kinetics. Therefore, the relationship between the mass ratio (α) and Φ (α) is defined as the MDC. MDC is unique for each powder and binder system, as described previously. **Figure 10**[84] is typical illustration of MDC developed for PIM feedstock based on intrinsic kinetics of polymer pyrolysis. In addition, Enneti *et al.*[74] presents a detailed review article on major progress of the thermal debinding process in particulate materials processing. This study includes progress made in understanding various phenomena during polymer burnout from PIM molded parts, focusing on a substantial reduction in thermal debinding time.

1.16.3.4 Sintering Process

In PIM, sintering is the fourth and final processing step. It is used to produce high-density parts with good mechanical properties. According to German,[85] sintering is a thermal treatment for bonding particles into a coherent, predominantly solid structure via mass transport events that often occur on the atomic scale. In addition, depending on the formulation and design of the binder system, the likely residues after the debinding process and pores left in the brown part are completely removed at this stage. Less attention is given to the debinding residues, which could be a serious issue for structural and/or magnetic effects of the finished part. The sintering process is identified as the processing stage that influences mechanical properties and other quality characteristics of the finished part.[77] At this stage, approximately 17–22% of shrinkage as well as other processing part defects become visible and pronounced. Therefore, it is important to handle the process with a robust design of experiment (DOE) to determine the optimum operating conditions. An optimum cooling rate of 10 °C min^{-1} was determined for both the mechanical properties and corrosion resistance of the sintered 316L stainless steel part, considering temperature, time, heating rate, and cooling rate as processing parmeters.[86] However, it is important to note that hardness and strength are the two mechanical properties commonly used to track finished part quality.

Typical processing parameters of the sintering operation are temperature, particle size, time, and pressure; the degree depends on the material properties. Although it is important to note that many materials densify as part of sintering, not all sintering involves densification. The process is characterized as pressure-assisted or pressureless sintering techniques.[85] Also, during the debinding (thermal debinding) and sintering processes, the green and brown parts are subjected to subsequent heat treatments, as depicted in **Figure 11**.[87]

The capability of PIM as a net-shaped microfabrication technique to produce parts with shiny and high surface finish values gives the technology a unique feature and makes it stand out among other microfabrication processes. This advantage is achieved through a number of factors: high density must be achieved and the metal surface must be free from reaction with sintering atmospheres to avoid the formation of oxides, nitrides, or other products. Consequently, the oxygen content or dew point in the atmosphere must be sufficiently low, and the amount of hydrogen or the degree of vacuum must be sufficiently high to reduce the metal oxides on micrometal parts surfaces. All these factors are considered to produce defect-free parts. Postprocessing of the finished part is implemented, but this strongly depends on target application. **Figure 12** illustrates tensile specimen parts at various processing stages of niobium powder injection molding, which depicts the advantages of multistep debinding techniques.

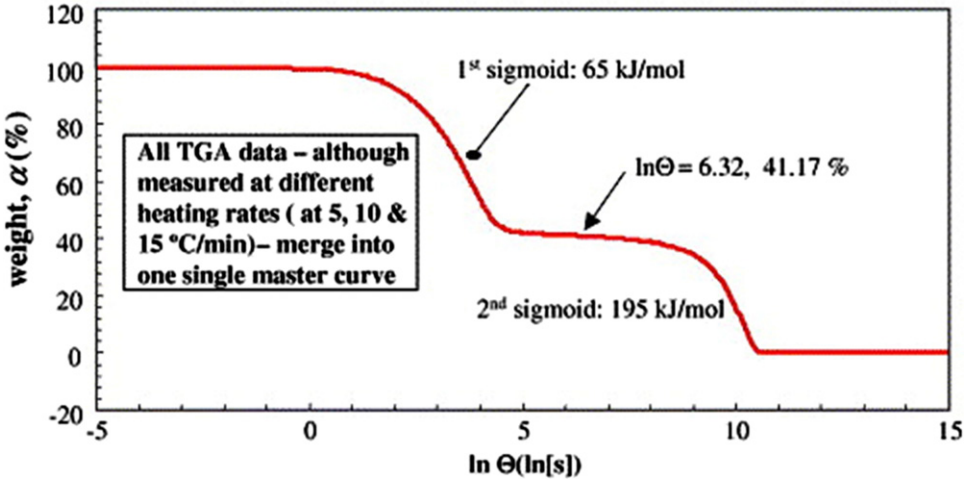

Figure 10 MDC of 57 vol.% of Nb solid loading feedstock. Aggarwal, G.; Smid, I.; Park, S. J.; German, R. M. Development of Niobium Powder Injection Molding. Part II: Debinding and Sintering. *Int. J. Refract. Metals Hard Mater.* **2007**, *35*, 226–236.

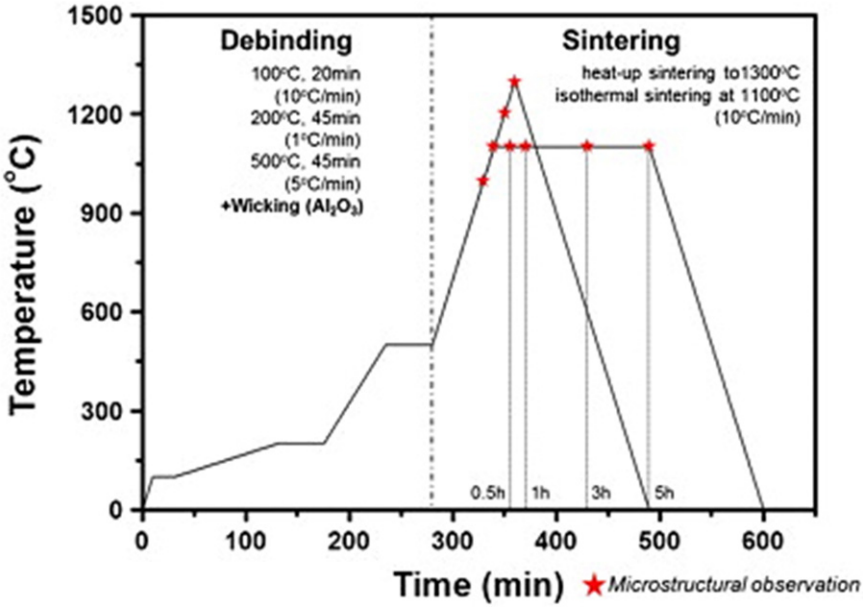

Figure 11 Typical heat treatment cycle during debinding and sintering processes of the molded part. Choi, J.-P.; Lee, G.-Y.; Song, J.-I.; Lee, W.-S.; Lee, J.-S. Sintering Behavior of 316l Stainless Steel Micro–Nanopowder Compact Fabricated by Powder Injection Molding. *Powder Technol.* **2015**, *279*, 196–202.

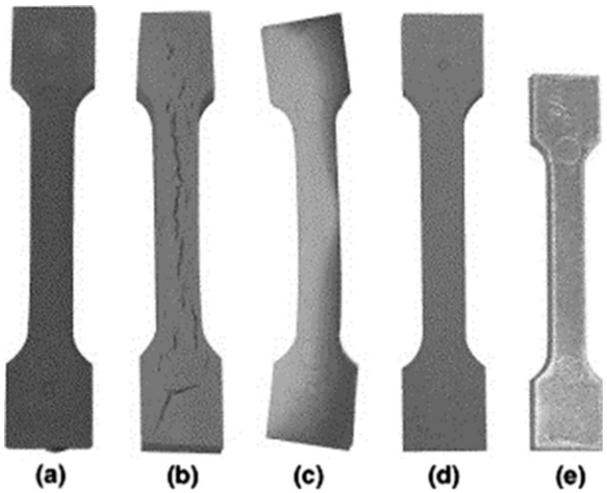

Figure 12 Niobium powder injection molding of tensile specimen and various processing products: (a) green part; (b) brown part by thermal debinding only; (c) brown part by solvent debinding followed by thermal debinding in nitrogen atmosphere; (d) brown part by solvent debinding followed by thermal debinding in argon atmosphere; and (e) defect-free finished part after sintering. Aggarwal, G.; Smid, I.; Park, S.J.; German, R. M. Development of Niobium Powder Injection Molding. Part II: Debinding and Sintering. *Int. J. Refract. Metals Hard Mater.* **2007**, *25*, 226–236.

1.16.4 Optimization and Simulation of Microinjection Molding Process

Product quality is improved by the application of optimization techniques to the manufacturing processes. These optimization techniques were developed based on global search process, statistical, and mathematical approximation. A broad classification of optimization techniques applied by researchers to injection molding process is presented in **Figure 13**.

A survey of literature as depicted in **Figure 13** shows that optimization techniques applied in injection molding process are classified as: intelligent algorithms,[88–91] iterative,[88,92–95] and noniterative[96–98] methods. In addition, a simulation-based classification of optimization techniques for IM is presented in **Figure 14**.[53] This consists of two broad categories: the direct discrete optimization and metamodel-based optimization methods. The metamodel-based method is further classified as response surface methodology (RSM), radial basis function, artificial neural network (ANN), and Kriging.

However, numerical simulations are sometimes integrated with DOE as optimization techniques to enhance product quality. The DOE approach is implemented to study the impact of processing parameters on quality characteristics such as strength, surface finish, part weight, shrinkage, and warpage of the finished part. These quality characteristics have been investigated to determine the optimum processing conditions of the microinjection molding process for different materials using the DOE approach. Zhao *et al.*[10] used DOE and considered the effect of five processing parameters on the microinjection molding process and quality of microgears. Various investigations based on DOE were performed to focus on determining optimal operating conditions[99–101] and quality characteristics of molded parts.[102–104] It is important to identify and control some key parameters that influence finished part quality in injection molding processes.

1.16.4.1 Parameter Control in Injection Molding Processes

It is important to control and monitor the injection molding process. IM is a repetitive process that requires close monitoring of many variables and parameters. Production consistency and

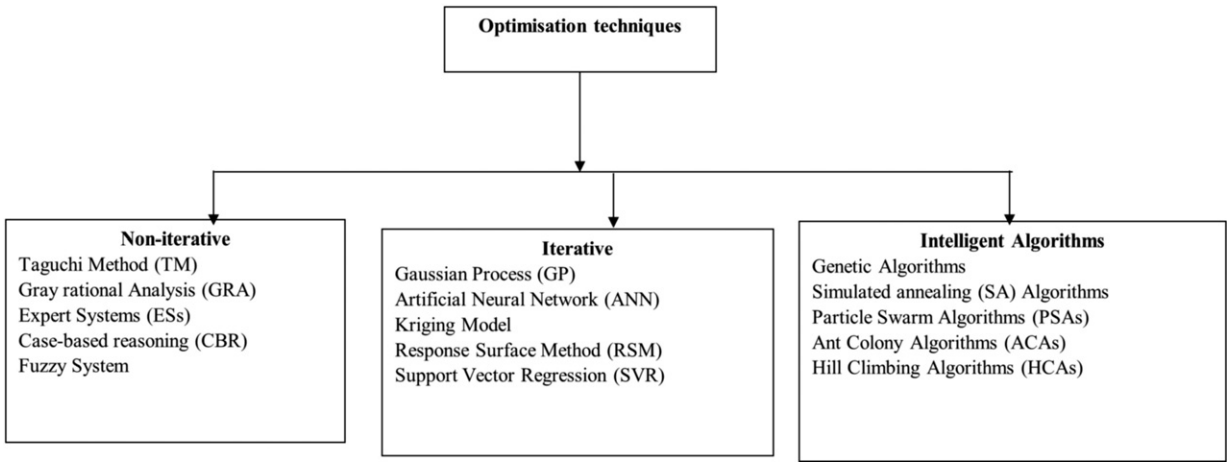

Figure 13 Optimization techniques used for IM process.

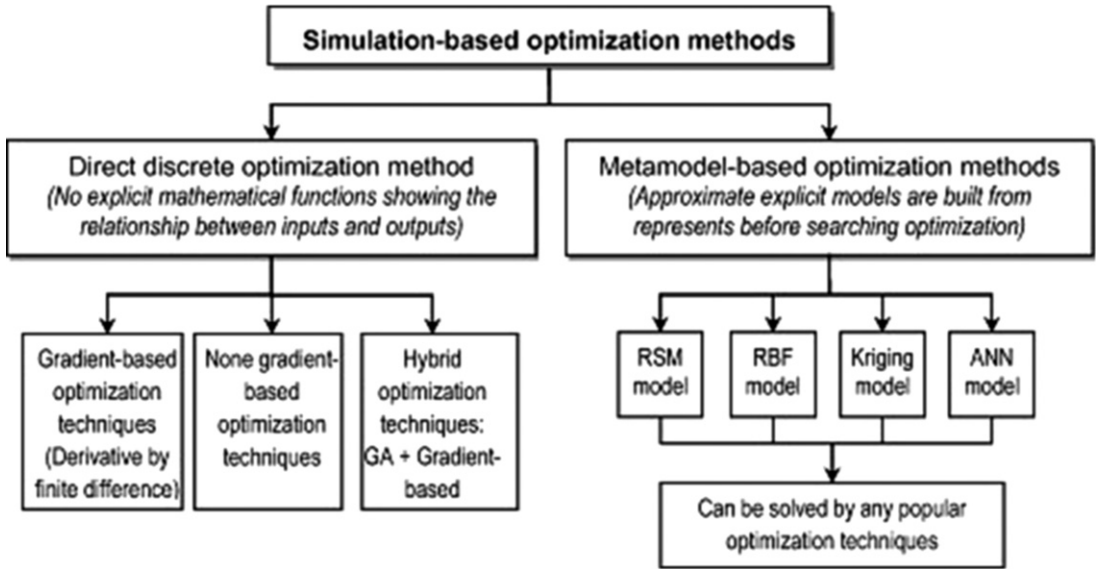

Figure 14 Simulation-based optimization techniques for IM. Dang, X.-P. General Frameworks for Optimization of Plastic Injection Molding Process Parameters. *Simul. Model. Pract. Th.* **2014**, *41*, 15–27.

part quality in IM are enhanced through control and monitoring of process parameters and conditions. IM is a very complex process that involves a high degree of interaction between feedstock material, machine, and process conditions. Therefore, the optimal performance of the IMM is characterized by production consistency and repeatability of the mold cycle. Therefore, precise control and monitoring of the processing conditions are necessary for efficient performance of IMM. However, not all parameters can be controlled and monitored at the same time. Some important parameters are linked directly to molded part quality. A typical control system in the modern injection molding process has the following main functions:

- manipulation of machine operational sequence control
- control of process and/or machine variables
- monitoring of process and performance evaluation status of the machine
- quality control of product to ensure consistency.

The sequence control ensures the molding machine operates according to the predetermined order and implements defined logic to provide target functions based on the circuit or tasks as specified in the software. This is an important function, but it does not directly influence product quality. The consistency of part quality from one production batch to another is a serious challenge in the IM process. In fact, sometimes the problem is experienced within batch production from one cycle to another, especially when manually operated or controlled. Then, process control and automation of machine operations become necessary to maintain

production consistency of parts. It is necessary to outline some important factors or key variables of the process, including process variables, material variables, and mold design variables, as presented in Table 11.

Therefore, the extent of the variability encountered by the machine output during operations is an indication of the level of inherent stability of the production. Hence, the smaller the variation, the more consistent and stable is the process.

Control and monitoring of the IM process provide continual support toward achieving a higher level of technology implementation to meet performance demands at the lowest cost. The control systems for the IM process available at present include closed loop (feedback) control, open load control, learning control, and advanced control. In addition, monitoring of the IM process is focused on statistical process control, multivariate statistics, and multiphase statistical process control. The functions of the control in injection molding are manipulation of machine sequence/mold cycle, control of machine variables, monitoring of process status and performance, and quality control of product/molded part. In addition, the control system is a useful tool for performing supervisory functions, process monitoring, and online evaluation of process variables statistically that can be used to alert the operator of any potential problems.

Table 11 Some processing variables of injection molding

Variable	*Factor/properties*	*Parameter*
Operating variables	Temperature	Melt temperatures Barrel temperature Nozzle temperature Mold temperature Cooling medium temperature
	Pressure	Injection pressure Holding/packing pressure Hydraulic back pressure Nozzle pressure Mold clamping pressure/force
	Time	Injection time Holding/packing time Pause (dwell) time Cycle time Cooling time
	Speed	Mold opening and closing mechanism speed Screw/ram speed Screw/ram recovery speed Component retraction spee
Material variables	Physical properties	Shear rate Shear stress Thermal conductivity Thermal diffusivity Specific volume Specific heat Viscosity Density
	Mechanical properties	Tensile strength Tensile modulus Elongation Compressive strength Compressive modulus Flexural strength Flexural modulus Impact strength Hardness Tensile creep Flexural creep Tensile fatigue Flexural fatigue
Mold design variables	Mold cavity measurements/ dimensions	Part dimensions and tolerances Cooling channel size Venting channel size Gate(s) location and size Runner system design

Some key variables that are often controlled in the IM process that allow optimum machine output are enumerated as temperature, pressure, injection velocity, and screw speed control. A typical experimental setup for monitoring and control of variables such as melt temperature, barrel temperature, nozzle temperature, and screw speed is illustrated in Figure 15.[105]

Figure 15 is a typical example of experimental setup of the control structure featuring SM25 IMM by Jhen-Syong Company, as reported by Lin and Lian.[105] Multiple sensors are used for data acquisition systems during operation to monitor various changes of both processing parameters and quality of the molded part. Many researchers have investigated the injection molding process by using sensors for measured variables such as injection pressure, cavity pressure, displacements and velocity of the injection pin, mold temperature, clamping, and demolding force.

1.16.4.2 Optimization Methods

The application of optimization methods in the injection molding process has become popular among researchers as they explore ways to improve quality of molded parts. The quality of molded parts is described in terms of quality characteristics, including physical and mechanical properties of dimensional conformity, surface finish, strength, hardness, and microstructure morphology. Part quality is affected by many variables and factors that are influenced by the process conditions of injection molding. This, in turn, gives rise to many processing parameters of injection molding that need to be monitored and controlled to achieve the desired molded part quality. Then, the need for selecting appropriate input variables and response factors becomes necessary. Based on this requirement, researchers applied the method of trial and error to investigate the effect of process parameters on the quality of characteristics. This involves choosing one parameter at a time and observing its effect on molded part quality characteristics of interest.

However, this technique is useful but not economical; it wastes time and materials. Due to this shortcoming, there was a shift to the DOE. The DOE technique considered the effect of more than one parameter at a time on specified quality characteristic of the molded part. This approach is widely accepted and adopted for investigation of processing parameters in microinjection molding. Table 12 presents a summary of the DOE technique as applied to microinjection molding process investigations and corresponding statements of the research findings for various materials.[101,106]

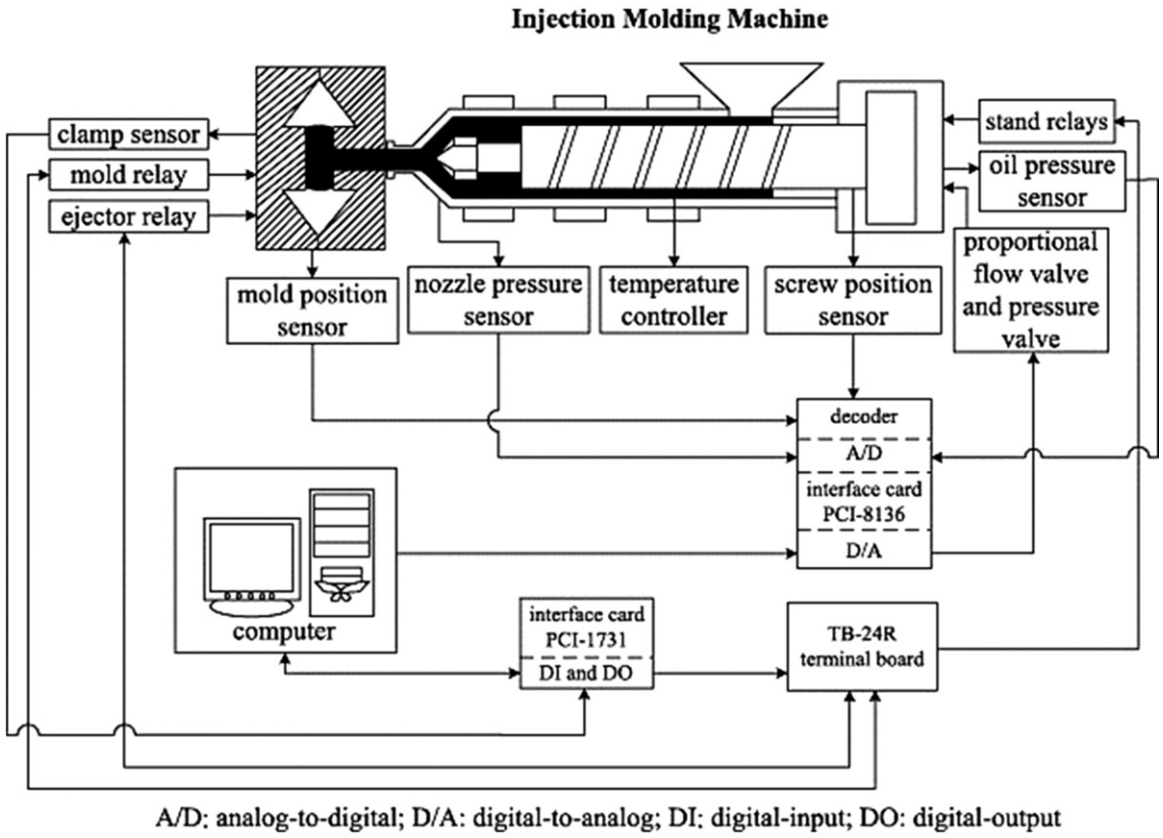

Figure 15 Experimental setup of control system for IMM. Lin, J.; Lian, R.-J. Self-Organizing Fuzzy Controller for Injection Molding Machines. *J. Process. Contr.* **2010**, *20* (5), 585–595.

The approach of DOE is most suitable for consideration of a few variables. However, as the number of variables increased, the techniques became cumbersome and the need for a more robust experiment design became required. Therefore, the method of optimization is then used for investigation of the processing conditions and the response factor(s).

The intelligent algorithms are optimization methods that are based on a global search process in a given design window. Meanwhile, long computational times are required for the simulations, which are based on black-box software. Likewise, the iterative methods are based on the approximate mathematical function obtained by a surrogate model constructed by running a simulation code. The most well-known surrogate models are the RSM, Kriging model, Gaussian process, ANN, and support vector regression. The third category is the non-iterative, with techniques that involve searching for optimum process conditions. This category includes the expert systems, gray relational analysis, fuzzy systems, case-based reasoning, and Taguchi method. In terms of product quality, the Taguchi method is widely used; therefore, some details of this method are outlined here. The Taguchi method is based on a robust design that requires the minimum cost of material and time for experiments and/or simulations.

In recent years, application of the Taguchi method has been proven to be efficient for product quality improvement.[100] However, the Taguchi method is outstanding because it centers on improvement of quality characteristics and integrates engineering and statistical methods to provide high-quality products at minimum cost. The method is based on robust DOE and is implemented by orthogonal array (OA), signal-to-noise (S/N) ratio, and analysis of variance.

The uniqueness of the Taguchi method is the design of OA. The OA responses are obtained via running the simulation code or performing corresponding experiments. OA can be divided into several classes: full level, two levels, and three levels; it is expressed as $L_n(x^y)$, where n is number of runs and x and y represent the level and number of factors considered. **Table 13** is an illustration of the OA design that features $L_9(3^4)$.

Empirical data are evaluated based on three criteria for optimized quality: the more nominal the better; the smaller the better; and the higher the better; the quality characteristics are continuous for engineering analysis. The mean-square deviation for these three quality characteristics can be expressed as:[107]

The more nominal the better:

$$\mathrm{MSD} = \frac{\bar{y}^2}{S^2} \qquad [43]$$

The smaller the better:

$$\mathrm{MSD} = \left(\frac{1}{n}\sum_{i=1}^{n} y_i^2\right) \qquad [44]$$

Table 12 Application of design of experiment for the investigation of molded part quality

Materials[a]	*Number of variables*	*Factors*		*Finding*
		Controlled	*Response*	
PC, SBS, MABS, COC, and PMMA	6	Melt temperature, injection pressure, holding pressure, injection speed, and mold temperature	Filling quality of microfeatured channels	Melt temperature and mold temperature are most significant parameters
PS, PC, and PMMA	5	Injection time, injection pressure, injection temperature, and mold temperature	3D numerical simulation of part filling	The mold temperature is the most important parameter; it must be higher than material T_g
PC and POM	6	Injection speed, holding pressure time, metering size, melt temperature, and mold temperature	Part weight and dimensions	Metering size and holding pressure are most significant; the interaction between both is also important
PS and PC	5	Injection speed, mold temperature, melt temperature, and holding pressure	Complete filling of donut-shaped parts	Injection speed and holding pressure are the most influential, whereas melt temperature and mold temperature have less influence
PP, POM, and ABS	7	Melt temperature, mold temperature, injection speed, holding pressure, air evacuation, and the size of features	Complete filling of high-aspect-ratio rods	Melt temperature and injection speed are key factors for PP and ABS; mold temperature is also significant in case of POM
PC	6	Injection speed, shot size, vacuum, holding pressure, piston diameter	Microfeature height	The diameter of the piston, shot size, injection speed, and mold temperature are significant parameters
PP, POM, and ABS	5	Melt temperature, mold temperature, injection speed, and distance between microfeatures	Complete filling of microstructures	Injection speed and melt temperature are influential in cases of POM and ABS with some side effects; mold temperature improves filling for some shapes; distance between microfeatures is not influential
PP, ABS, and PC	5	Melt temperature, mold temperature, injection speed, and surface finish	Flow length along a micro-channel into a flat cavity	The high levels of all processing parameters result in better filling; surface finish is related to level of turbulence in melt flow
PS	5	Melt temperature, mold temperature, injection speed, and holding pressure	Weld-line formation	Injection speed and mold temperature have the main effect on weld-line placement and orientation
PP	5	Injection pressure, melt temperature, mold temperature, and flow ratio	Flow length	Melt temperature and injection pressure are the most significant factors
COC	4	Holding pressure, filling flow rate, and mold temperature	Filled volume fraction of microfilters	Flow rate found to be the most important processing parameter

[a]Polycarbonate (PC); styrene-butadiene-styrene (SBS); methylmethacrylate acrylonitrile-butadiene-styrene (MABS); cyclic olefin copolymer (COC); polymethylmethacrylate (PMMA); polyoxymethylene (POM); acrylonitrile-butadiene-styrene (ABS); polypropylene (PP); polystyrene (PS).

Source: Modified from Attia, U.; Marson, S.; Alcock, J. Micro-Injection Moulding of Polymer Microfluidic Devices. *Microfluidics and Nanofluidics* **2009**, *7* (1), 1–28; From Attia, U. M.; Alcock, J. R. Optimising Process Conditions for Multiple Quality Criteria in Micro-Injection Moulding. *International Journal of Advanced Manufacturing Technology* **2010**, *50* (5–8), 533–542.

The higher the better:

$$\mathrm{MSD} = \left(\frac{1}{n}\sum_{i=1}^{n}\frac{1}{y_i^2}\right) \quad [45]$$

where $\bar{y}$ is the mean of the sample, S is the standard deviation, y_i is the response value for the specified problem in the ith test, and n is the number of replications in each test trial. Regardless of the category of the quality characteristics, a higher algebraic value of the S/N ratio corresponds to better quality characteristic, such as the smaller variance of the output characteristic around the desired (target) value. The S/N ratio for either of these mentioned criteria is evaluated using eqn [46] with a unit of dB.

$$\eta = S/N = -10\log(\text{MSD}) \quad [46]$$

Therefore, the application of the Taguchi[108,109] optimization method based on multiple quality characteristics of IM continues to emerge as the approach to minimize cost, time, and variation of production processes. This has increased performance and productivity of a given process or system, and improves part quality. Figure 16 illustrates the flow sequence of the Taguchi method.

1.16.4.3 Application of Computer Modeling in Injection Molding Processes

Simulation of the MIM process is quite complex and involves nonisothermal, non-Newtonian flow of shear-thinning of the two-phase fluid flow. The principles were adopted from early developments made in plastic injection molding simulation codes and software based on the Hele–Shaw model. These software solutions are implemented by discretization methods such as finite difference method (FDM), finite volume method (FVM), and finite element modeling (FEM) methods. Newer methods such as the mesh-free method have been developed to eliminate issues with mesh and element grids.

The process design of microinjection molding involves the determination of a number of processing parameters such as pressure (injection, holding, and melt), temperature (coolant, nozzle, barrel, melt, and mold), time (fill, holding, cooling, and cycle), clamping force, injection speed, and injection stroke. In such process, due to the irregular geometry in microscale and the complex thermo-mechanical history during the injection molding cycle, it is generally necessary to resort to numerical simulation methods to properly simulate the molding process and develop the capability of predicting the final configuration of the molded part. The target goals of adopting simulations in the injection molding process by researchers are summarized under the following heading[71, 106]:

i. Flow visualization and prediction of the mold cavity filling during injection molding process. The focus is on the material properties of the melt and tooling geometry on flow and the filling of mold cavity. The objective includes monitoring incomplete filling of the mold cavity and determination of part defects such as weld line and voids, which depend on the runners and gate location of the mold design.
ii. Parametric design analysis and optimization of the part and mold cavity design. This includes the virtual geometry analysis of the mold cavity in relation to the shape of the parts to be produced. This eliminates cost of reconstruction and early identification of a likely problem if trial-and-error methods were used. In addition, the technique will determine and establish optimum mold design and operating conditions.

Table 13 $L_9(3^4)$ Taguchi orthogonal array

Run	*P_1*	*P_2*	*P_3*	*P_4*
1	1	1	1	1
2	1	2	2	2
3	1	3	3	3
4	2	1	2	3
5	2	2	3	1
6	2	3	1	2
7	3	1	3	2
8	3	2	1	3
9	3	3	2	1

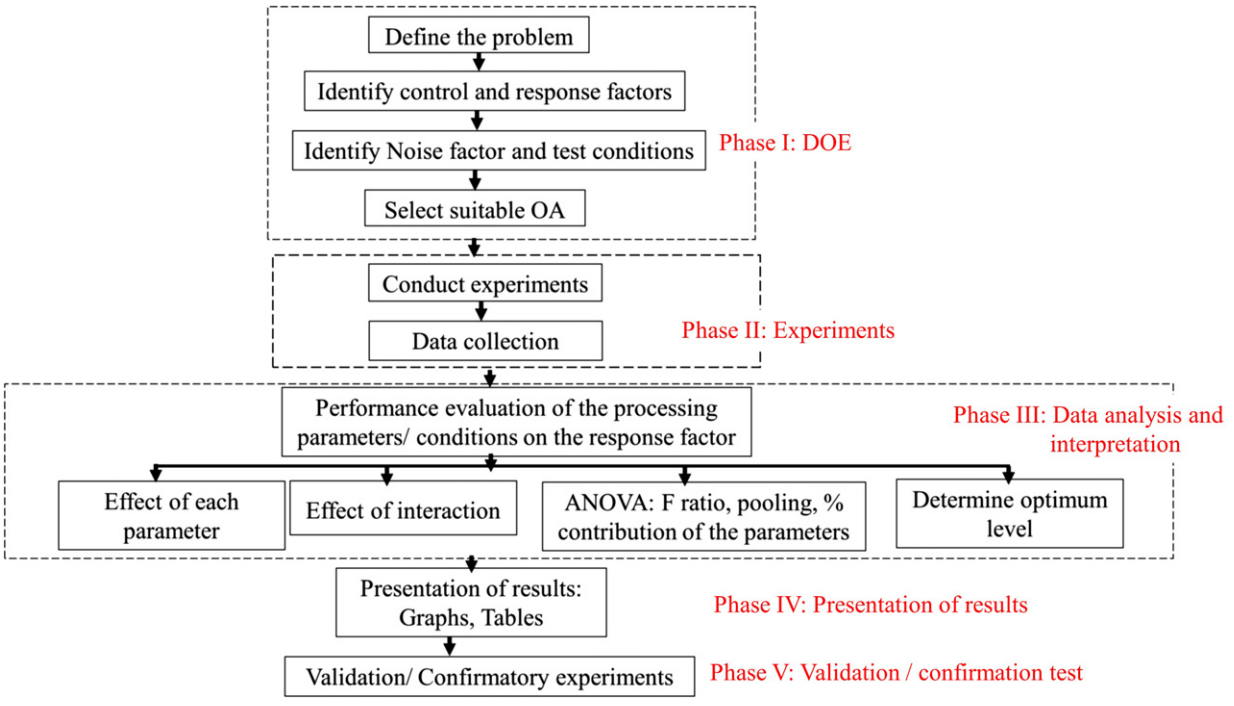

Figure 16 Operational sequence of the Taguchi method.

iii. Modeling of the material properties such as thermal, residual stresses, specific heat coefficient, and processing conditions of melt flow during filling and cooling, which would be useful in estimating the cycle time and determining the critical processing variables and factors.
iv. To identify postprocessing properties and factors, which influence finished part quality characteristics such as shrinkage, warpage, weight, density, and surface finish.
v. To measure and validate empirical data such as warpage and volumetric shrinkage of the part, which are not easily determined experimentally. These quality characteristics are monitored through computer simulation, some of which influenced quality of the finished part.

Despite success of the simulation techniques in micro-injection molding, several factors affect the accuracy of model results.[71] Peter and Rong[110] generalized the complications as:

i. the nature of injection molding, particularly the basic physics of the process
ii. the properties of the material
iii. the geometric complexity of the mold.

1.16.4.3.1 Developments in the simulation of injection molding process

There are several milestones in the history of computer aided engineering (CAE) applications for injection molding. The history of simulation and computer software development are described in detail by Peter and Rong,[110] Zheng *et al.*,[111] and Zhou.[112]

According to Liu *et al.*,[41] computer simulation is used to reduce the design-to-manufacture cycle time through optimization of both design and process parameters. A survey of literature indicates that melt temperature, mold temperature, holding pressure, injection pressure, and injection speed were mostly investigated; these parameters directly influenced part quality.[113] Other factors such as material properties, powder loading, and surface finish of the mold may influence part quality. Therefore, software and codes are developed to predict quality characteristics of products in IM. For some quality characteristics, properties and/or factors are not easily measurable experimentally.[105,114] Several commercial software programs such as ANSYS CFX, PIMSolver, SIGMASOFT, CMOLD, Moldex3D, Moldflow, Solidworks plastics, and others are widely used for injection molding simulations.[115] Some of these software programs were originally developed to handle convectional injection molding and other applications. With little modification to the simulation setup, the software is found to very useful for the prediction of quality characteristics of μIM molded parts.

1.16.4.3.2 Computer simulation and molded part quality enhancement

Computer simulation has significantly supported the development of μPIM, starting from the use of applications and codes developed for plastic injection molding. Many studies have been conducted and various findings reveal a better understanding of the technology. The simulation is used for the determination of optimum operating conditions of the process, the inter-relationships, and correlation among parameters. A survey of the literature indicates that application of computer modeling for enhancement of molded part quality in μIM could be categorized into three phases: simulation, optimization, and process control and monitoring, as depicted in Figure 17.

Today, computer applications in PIM are used extensively beginning from part drafting, which involves computer-aided drafting, and sometimes the process is implemented in CAE. CAE is a very wide field of computer applications including finite element analysis, computational fluid dynamics (CFD), multibody dynamics (MBD), and optimization. In addition, optimization in μIM includes both the design and process, as shown in Figure 17. The design aspect of the optimization is the parametric analysis of the virtual part to be produced to determine appropriate part dimensions, shrinkage factors, and other design variables considered. The application of various optimization techniques to determine optimum operating conditions from the process variables is also considered. This aspect has been described in Section 1.16.4.2. Then, the control and monitoring of defect-free parts is to ensure quality variables through the process of machine execution. This is connected to monitoring and control of finished part quality characteristics.

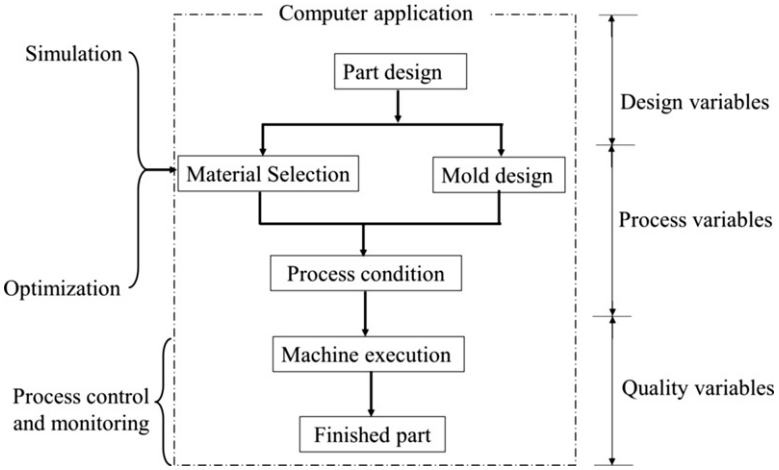

Figure 17 Application of computer modeling for quality enhancement of molded parts in μIM.

However, it is important to investigate the process condition and to establish the influence of process parameters on the quality characteristics of the molded or finished part in μIM. Prior to experimental setup, researchers used computer simulation to investigate the material properties, melt flow into mold cavities (runners and gate). The simulation analysis includes three phases (the filling, packing/holding, and cooling phase) of μIM process.

1.16.4.3.3 Modeling of injection molding process

The success of a defect-free part in μIM depends strongly on the ability of the feedstock melt to flow into the mold cavity for microstructures and nanostructures.[116] Lin *et al.*[117] examined the effects of the processing parameters on the filling of nano feature components through the development of analytical models that were verified and validated experimentally. Their finding indicates that nanoscale filling requires higher mold temperatures. However, whenever the filling aspect ratio is more than 1, the mold temperature should be raised near or above the glass transition temperature of the polymer. The suitability of analytical methods diminishes as the complexity of the microfeature/molded part increases, thus giving rise to the use of numerical methods. Modeling and mathematical derivations have been implemented by the application of suitable numerical methods to solve the governing equations developed or formulated for injection molding simulation.[118–121] These governing equations are formulated to consider the operational condition as well as the material properties of the feedstock.

1.16.4.3.3.1 Feedstock properties and mixing simulation

The material properties of the feedstock considered for injection molding simulation depend on many factors and processing conditions. Thus, rheological investigations of the feedstock are essentially studied for the analysis of melt flow behavior during mixing and injection (filling, packing, and cooling phase) of molded part modeling. Some of these properties considered are viscosity, shear modulus, specific heat capacity, elastic modulus, thermal conductivity, and pressure–volume–temperature (PVT), among others. A general rule-of-mixtures model for some of these properties is presented in Section 1.16.3.1.3. Due to the importance of viscosity and availability of models, it is further discussed here. For the model injection molding process, a viscosity model (function) is required to predict the fluid flow behavior. The viscosity curves of most thermoplastics and polymeric binders used in the PIM process have the same dependence on shear rates. The viscosity hardly changes when the rate of shear is very low or very high; at this time, pseudoplastic fluid acts similar to a Newtonian fluid. At least four parameters are required to reflect this relationship between viscosity and shear rate.

Modeling of viscosity has attained remarkable landmarks by models proposed by Cross[122] in 1965 and Carreau[123] in 1972, respectively. These models are believed to be better than the others in terms of representation of characteristics of the thermoplastic polymer investigated. In addition, the Sisko model[124] proposed by Sisko in 1958 combined the characteristics of Bingham plastics and the power law model. Models such as the Prandtl–Eyring model, Ellis model, Casson model, and fractional exponential model are developed for other specific applications. Currently, the power law and the cross model are widely used in injection molding to describe the viscosity function.[125] Therefore, an overview of these models and the mathematical relationship is presented.

1.16.4.3.3.1.1 Power law model

This is a well-known viscosity model that is often used in most injection molding simulations. de Waele in 1923 and Ostwald in 1925 proposed the power law model,[122] also known as the Ostwald–de Waele relationship, which has been used successfully to predict the shear thinning region. This model has the following form:

$$\eta = \eta_0 |\dot{\gamma}|^{n-1} \quad [47]$$

$$\eta_0 = B\left(\frac{T_b}{T}\right) \quad [48]$$

where η_0 is the Newtonian viscosity or zero shear rate viscosity, which is defined as the viscosity at zero shear rate, B is a constant called the consistency index, T_b is a constant showing the temperature sensitivity of this material, T is the melting temperature, and n is the power law index with a value between $0 < n \geq 1$ for polymer melts. The natural logarithms of the eqn [48] give:

$$\ln(\eta) = (n-1)\ln(\dot{\gamma}) + \ln(\eta_0) \quad [49]$$

Flow behaviors of a power law fluid depend on the value of n[126] for:

$n < 1$, the fluid exhibits shear-thinning properties;
$n = 1$, the fluid shows Newtonian behavior;
$n > 1$, the fluid shows shear-thickening behavior.

According to Thavanayagam *et al.*,[37] feedstocks that exhibit shear thinning ($n < 1$) are suitable for PIM. Feedstock with dilatant flow behavior ($n > 1$) is not suitable for PIM because powder and binder separation can occur under a high shear rate. Therefore, rheological properties should be assessed over a wide range of shear rates.

Equation [49] is termed the first-order viscosity model and used in Moldflow software for flow analysis of the injection molding process. To improve the modeling of viscosity in the low shear rate region, the second-order model was developed by Moldflow and expressed as:

$$\ln \eta = A_0 + A_1 \ln \dot{\gamma} A_2 T + A_3 (\ln \dot{\gamma})^2 + A_4 T \ln \dot{\gamma} + A_5 T^2 \quad [50]$$

where A_i are constants and T is temperature. According to Koszkul and Nabialek,[127], this model has been criticized on the grounds that it is based on empirical observations. This is of little relevance for our purposes. What is required is a model that fits the experimental data as closely as possible, and the second-order model is able to characterize the observed behavior of polymer melts. In particular, the second-order model can model the following features of polymer melts:

a. convergence of iso-shear rate curves with increasing temperature,
b. convergence of isotherms with increasing shear rate,

c. the increasing rate at which viscosity decreases as shear rate is increased,
d. the increasing rate at which viscosity decreases with increasing temperature.

In general, the literature demonstrates that the power law represents the behavior of polymer melts in the high shear rate region, and it is also quite easy to fit experimental data for the model and determine the constants η_0 and n. In the Moldflow simulation software, the first is developed based on empirical data. The second model is used to characterize the behavior of the melts. However, the main disadvantage of the model is in the low shear rate range. Despite this shortcoming, the model has been widely used for modeling flow in injection molding. It is important to consider the phase of the process under consideration independently. For instance, particularly in the filling phase, shear rates are frequently high enough to justify the use of the first-order model. Shear rates are often low in the packing phase. Also, it is possible to have low shear rates in the filling phase when the filling pattern is unbalanced.

1.16.4.3.3.1.2 Cross Model

The cross viscosity model is expressed as:

$$\eta = \frac{\eta_0}{1 + \left(\frac{\eta_0|\dot{\gamma}|}{\tau^*}\right)^{n-1}} \quad [51]$$

where τ^* is the shear stress at the transition between Newtonian and power law behavior, which can be modeled using the widely accepted seventh constant cross model

$$\eta_0 = D_1 \exp\left[-\frac{A_1(T - T^*)}{A_2 + (T - T^*)}\right], \quad A_2 = A_3 + D_3 P, \quad \text{and} \quad T^* = D_2 + D_3 p \quad [52]$$

where η_0, n, τ^*, and $\dot{\gamma}$ denote the zero heat rate viscosity, the power law index, the critical stress level at the transition to shear thinning, and the shear rate. T^* is the glass transition temperature, p is the pressure, and A_1, A_2, A_3, D_1, D_2, and D_3 are data-fitted coefficients.

Compared to plastic injection molding, PIM is more prone to IM defects such as jetting and nonuniform flows, and both PIMSolver and Moldflow are useful simulation software for predicting injection molding filling defects. However, a follow-up with experiments is highly recommended, especially for PIM. Concentrated powder/binder mixtures have a peculiar nature of yield stress with shear-thinning viscous behavior. To be able to simulate these natures, the modified cross model for viscosity as a function of the effective shear rate and temperature is used for PIMSolver.

$$\eta(\dot{\gamma}, T) = \frac{\eta_0}{1 + C(\eta_0 \dot{\gamma})^{1-n}} + \tau_y \dot{\gamma} \quad [53]$$

where η_0, n, τ^*, and Tb denote the zero shear rate viscosity, the power law exponent, the transition shear stress, the constant amplitude, and the reference temperature in absolute scale for the Arrhenius temperature dependence of the viscosity. A new term τ_y is added to the modified cross model in eqn [53] for the yield stress.[128,129] Equation [56] is a viscosity model developed by PIM specialists for PIMSolver software.

1.16.4.3.3.1.3 Carreau model

The Carreau model has the form:

$$\frac{\eta - \eta_\infty}{\eta_0 - \eta_\infty} = [1 + (\lambda\dot{\gamma})]^{(n-1)/a} \quad [54]$$

where η_∞ is the viscosity at infinite shear rate, η_0 is the viscosity at zero shear rate, n is a dimensionless constant with the same interpretation as the power law model eqn [47], and K is a material time constant parameter. The Bird–Carreau model is given by $a=2$. For many shear thinning fluids, $a \approx 2$.

1.16.4.3.3.1.4 Ellis Model

The Ellis model presents the viscosity as a function of shear stress τ, mathematically represented as:

$$\frac{\eta_0}{\eta} = 1 + \left(\frac{\tau}{\tau_{1/2}}\right)^{\alpha - 1} \quad [55]$$

where $\tau_{1/2}$ is the value of shear stress for which $\eta = \eta_{0/2}$ and $\alpha - 1$ is the slope of the graph $\ln[(\eta_0/\eta) - 1]$ versus $\ln(\tau/\tau_{1/2})$.

However, the research effort is still ongoing for a more suitable model for different material. Recently, Hidalgo *et al.*[35] proposed a generalized rheological model that involves the following parameters: shear rate (γ), temperature (T), solid loading (Φ), and particle size (PS). The model is expressed as:

$$\eta(\dot{\gamma}, T, \phi, \text{PS}) = \frac{C_u}{d_{50}} \cdot \exp\left(\frac{E_a}{\text{RT}}\right) \cdot \left(\frac{\tau}{\dot{\gamma}} + \left(\frac{\eta_0}{1 + K\dot{\gamma}^n}\right)\right) \cdot \left(\frac{\phi_{\text{crit}}}{\phi_{\text{crit}} - \phi}\right)^m \quad [56]$$

Having fully understood the properties of the metal powder, valuable information will be obtained from simulation of the mixing process.

1.16.4.3.3.1.5 Modeling of feedstock mixing

In practice, distributive mixing of feedstock constituents is investigated without concern for molecular diffusion. Although the behavior of melt during preparation is analyzed by fluid flow governing equations for specific mixer geometry for given material properties and operating conditions. Finite element method (FEM) is used mostly for the analysis of the governing fluid flow equation. According to Huang and Kuo,[130] computer simulation is a numerical tool that is more cost-effective than performing experiments in complex systems. This establishes a basis for design optimization, scale-up, and control of the system. Nevertheless, there are two common numerical approaches for studying particle mixing: the discrete approach and the continuum approach. The Monte Carlo method, cellular automata, and discrete element method (DEM) were developed based the on discrete approach. In addition, researchers now prefer to analyze granular flow with CFD because the continuum approach does not account for a system size relative to DEM. The flow pattern of mixing particles can be described as either dispersive or distributive mixing,[131] as illustrated in **Figure 18**.

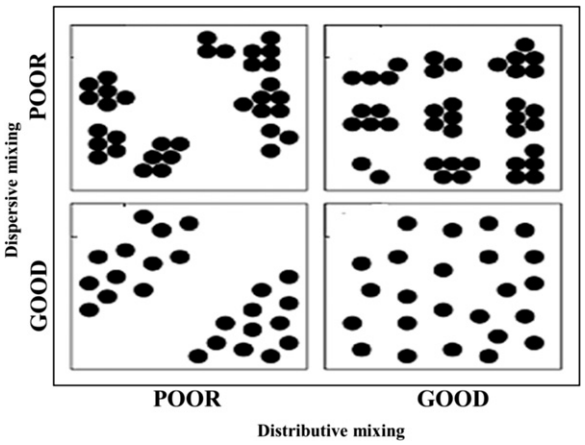

Figure 18 An illustration of dispersive and distributive mixing.

Therefore, the governing equations for the analysis of the feedstock melt during mixing are as follows:

$$\nabla \cdot \vec{V} = 0 \quad [57]$$

where $\vec{V}$ is the local velocity of the moving part

$$H(v - \vec{V}) + (1 - H)\left[\nabla \cdot \vec{\tau} - \nabla p + \rho\left(\frac{\partial v}{\partial t} + v \cdot \nabla \vec{V}\right)\right] = 0 \quad [58]$$

where H is a step function equal to 0 for fluid field and 1 for inner moving parts, v is the fluid velocity, $\vec{\tau}$ is the strain rate tensor, P is the fluid pressure, ρ is the fluid density, and t is the time.

$$\rho C(T)\left(\frac{\partial T}{\partial t} + v \cdot \nabla T\right) = T \cdot \nabla v + r - \nabla \cdot q \quad [59]$$

where $C(T)$ is the heat capacity as a function of temperature, r is volumetric heat source, and q is the heat flux.

Equation [57] is the continuity equation, eqn [58] is the momentum, and eqn [59] is the energy equation. The stress tensor and the shear rate are defined by eqn [60] and expressed as:

$$\vec{\tau} = 2\eta(\dot{\gamma}, T)\vec{D} \quad [60]$$

$$\dot{\gamma} = \sqrt{2\vec{D} : \vec{D}} \quad [61]$$

Suitable viscosity model is selected or developed from empirical data to describe the material behavior of the feedstock.

The equations formulated are solved by the numerical method, but the FEM is dominantly used. The particle tracking method has been successfully applied. Analysis of feedstock mixing by the particle tracking scheme involved three steps:

- flow analysis to obtain a velocity field of a mixing device;
- particle tracking step to obtain distribution of particles at the end of the mixer;
- quantification of mixing from the obtained particle distribution.

Then, to track the relative position of particles within a specified domain, the solution of the physical model involved is an ordinary differential equation (ODE):

$$\frac{dx}{dt} = u \quad [62]$$

where x is the particle position vector, u is the particle velocity, and t is the time. The numerical method is used for the solution of the 3D problem. These equations are sometimes simplified to 2D to save time and resources. The fourth-order Runge–Kutta method is widely used for solving eqns [62].

The homogeneity of the powder-binder mixture is evaluated by the mixing uniformity to achieve the required distribution of the particles. A proper measure of mixing is the uniformity of the particle distribution as well as information on material properties such as the entropy of the particles at any given cross-section within the mixing domain based on tracking method. The characterization of the mixing progress requires first the division of the mixer cross-section into a number of cells. Then, for a certain particle configuration, the mixing entropy S is defined as a sum of the information entropy of individual cells constituting the cross-sectional area, defined by:

$$S = -\sum_{i=1}^{N} n_i \log n_i \quad [63]$$

where N is the number of cells and n_i is the particle number density at the ith cell. Instead of directly using the information entropy in the mixing analysis, we use a normalized entropy. Increased S^* as a measure of mixing is given by:

$$S^* = \frac{S - S_0}{S_{max} - S_0} \quad [64]$$

where S_0 is the entropy at the inlet and S_{max} is the maximum possible entropy, defined by log$N$, which is the ideal case with a uniform distribution of the particles, such as $n_i = 1/N$.

1.16.4.3.3.2 Fundamentals of governing equations and boundary conditions

The governing equations are a set relationship describing the physical model or system. In typical fluid flow, the conservation equation of mass, momentum, and energy are expressed in a similar form. The mathematical representations of these equations are based on fundamental physical principles, on which all fluid flow is derived. However, formulation or choice of a suitable equation for the analysis of the fluid flow is very important and fundamental for CFD. When obtaining the basic equations of fluid dynamics, the following philosophy is always followed:

(1) The governing equations are derived from the fundamental physical concepts of physics, namely:
   - mass is conserved
   - conservation of momentum F = ma (Newton's second law)
   - energy is conserved.

(2) The fundamental physical concepts are applied to a suitable model to describe the fluid.

(3) Mathematical modeling for the fluid.

A suitable boundary condition is imposed on the ODE or partial differential equation (PDE). These conditions (such as slip, inertia, isothermal, isobaric, etc.) and specified values for the independent variable(s) such as temperature, pressure, and velocity over a range at which the solution being analytical or numerical is expected to converge.

1.16.4.3.3.3 Melt flow behavior in micro-size channel

The actual design of the runner is usually trapezoidal in the cross-section, which allows easy ejection of the part from the mold. However, most 2.5D mold-filling simulation software programs approximate the geometry of the channel to the circular cross-section runner. The graphical user interface of the software may provide various alternatives, but usually the black-box evaluation of the software approximates to an equivalent circular cross-section. This approach is not a satisfactory approximation and may introduce an appreciable error in computational results of the software. Therefore, there is a need for analytical modeling or in-house code to study the melt front flow behavior in microcavity filling of μIM.

The flow and filling analysis of the mold cavity during μIM by the feedstock melt has been investigated. In this analysis, a single point injection of melt is considered through the runner channel to the mold cavity. **Figure 19** is a schematic representation of the runner channel. It is important to note that some assumptions were made. The injection flow rate is considered to be constant during the filling process of the cavity and locally filled. Likewise, the volume in the part required is far smaller as compared to the main cavity. The amount of melt flow rate in the main cavity is assumed to be the same as the injection rate. For one-dimensional viscous flow, the momentum equation can be expressed as:

$$\frac{dp}{dx} = \frac{d}{d\gamma}\left(\eta \frac{du}{d\gamma}\right) \qquad [65]$$

where η is the viscosity and, for a power law fluid, can be written as

$$\eta = m_x \dot{\gamma}^{n-1} \qquad [66]$$

where $\dot{\gamma}$ represents the shear rate, m_x is the flow consistency index, and n is the power law index. The microinjection molded cavity feature is filled within a short period of time. Then, the temperature of the melt within the thickness (h) of the main flow path is assumed to be constant. The consistency index (m_x) can be expressed as:

$$m_x = m_o e^{-a_0(T_m - T_0)} \qquad [67]$$

where T_m is the melting temperature at the main cavity, and m_o, a_o, and T_o are material constants. To solve for the velocity of the flow (u), eqns [66] and [67] are substituted into eqn [65] and expressed as:

$$u = \left(\frac{1}{m_x}\right)^{\frac{1}{n}} \left(\frac{n}{n+1}\right) \left|\frac{dp}{dx}\right|^{\frac{1}{n}} \left[\left(\frac{h}{2}\right)^{\frac{n+1}{n}} - \gamma^{\frac{n+1}{n}}\right] \qquad [68]$$

and the injection flow rate (Q) across the cross-section of the flow channel is given by:

$$Q = \left(\frac{1}{m_x}\right)^{\frac{1}{n}} \left(\frac{2nw}{2n+1}\right) \left|\frac{dp}{dx}\right|^{\frac{1}{n}} \left(\frac{h}{2}\right)^{\frac{2n+1}{n}} \qquad [69]$$

Also, the pressure (P_o) at point o, as indicated in **Figure 19**, depends on the melt filled distance (x_o) from the point to the flow front, which is assumed to be constant across the thickness of the main cavity and expressed as:

$$P_o = \frac{2^{n+1}(2n+1)^n}{n^n} \frac{m_x x_o}{w^n h^{2n+1}} Q^n \qquad [70]$$

The melt velocity (V_x) along the flow path of the main cavity is expressed as:

$$V_x = \frac{dx}{dt}$$
$$\frac{dx}{dt} = \frac{Q_x}{wh} \approx \frac{Q}{wh} \qquad [71]$$

where w is the width of the channel and h represents the depth of the micro-size channel. It is assumed that the amount of melt into the channel is quite small, and Q_x represents the flow rate at the main cavity. Also, Q_x is approximately the same as the injection flow rate, Q. Then, evaluating eqn [71] to estimate the flow front from point o is expressed as:

$$x_o = \frac{Qt}{wh} \qquad [72]$$

From eqn [68], pressure drop can be estimated and evaluated using:

$$\frac{dp}{dx} = m_x \left(\frac{2nw}{2n+1}\right)^{-n} \left(\frac{h}{2}\right)^{-(2n+1)} Q^n \qquad [73]$$

Then, substituting for m_x in eqn [73], the pressure drop can be expressed as a function of both the melt flow filled distance x_0 and the temperature.

$$\frac{dp}{dx} = \left(\frac{2n+1}{nw}\right)^n \left(\frac{h}{2}\right)^{-(2n+1)} Q^n m_o e^{-a_0(T_m - T_0)} \qquad [74]$$

Integrating eqn [74] or substituting for m_x in eqn [70] yields an expression for pressure in terms of the material properties and as a function of the temperature.

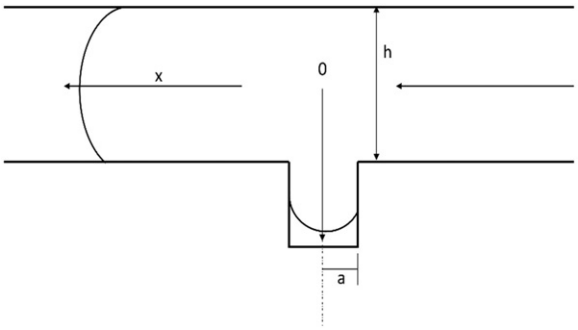

Figure 19 Schematics of the physical model for μIM flow channel.

$$p(x_0, T_0) = \left(\frac{2n+1}{nw}\right)^n \left(\frac{h}{2}\right)^{-(2n+1)} Q^n x_0 m_o e^{-a_0(T_m - T_0)} \quad [75]$$

Total pressure drop is a summation of the losses across the sprue, runner, and gate, as well as the within the mold cavity.

$$\Delta p = \Delta p_{\text{Pipe}} + \Delta p_{\text{cavity}} \quad [76]$$

Lin and Young[116] derived an analytical model for the estimation of pressure drop in the mold cavity as well as in the pipe. The combined effect of the pressure drop in the sprue, runner, and gate is referred to as Δp_{pipe} and expressed as:

$$\Delta p_{\text{Pipe}} = \left[\frac{2m_x(3n+1)^n \Delta x}{n^n \pi} R^{-(3n+1)}\right] Q^n = \overline{R}_{\text{pipe}} Q^n \quad [77]$$

where $\overline{R}_{\text{pipe}}$ is the hydraulic radius of the sprue, runner, and/or gate.

1.16.4.3.3.4 Filling phase of injection molding

The filling phase of injection molding is a very complex process. Its analysis is based on the generalized Hele-Shaw model with incompressible, generalized, non-Newtonian fluid under nonisothermal conditions. The governing equations of the feedstock melt are expressed as follows.

The continuity equation is expressed as:

$$\frac{\partial v_x}{\partial x} + \frac{\partial v_y}{\partial y} + \frac{\partial v_z}{\partial z} = 0 \quad [78]$$

The momentum equations are expressed as:

$$\frac{\partial p}{\partial x} = \frac{\partial}{\partial x}\left(\eta \frac{\partial u}{\partial z}\right) \quad [79]$$

$$\frac{\partial p}{\partial y} = \frac{\partial}{\partial y}\left(\eta \frac{\partial v}{\partial z}\right) \quad [80]$$

$$\frac{\partial p}{\partial z} = 0 \quad [81]$$

From eqn [78], V_x, V_y, and V_z represent velocity function along the x, y, and z axes, respectively, whereas p is the pressure and η is the viscosity. Most textbooks use u, v, and w for V_x, V_y, and V_z; these are only used for clarity. Then, combining eqns [78], [69], and [80] and integrating them along the z-direction (thickness direction) gives the fluid flow governing equation for the filling stage, expressed as:

$$\frac{\partial}{\partial x}\left(s\frac{\partial p}{\partial x}\right) + \frac{\partial}{\partial y}\left(s\frac{\partial p}{\partial y}\right) = 0 \quad [82]$$

$$s = \int_{-b}^{b} \frac{z^2}{\eta}\, dz \quad [83]$$

Based on the lubrication and Hele–Shaw approximations, the energy equation governing the mold cavity filling stage during injection molding by the melt is express as:

$$\rho C_p \left(\frac{\partial T}{\partial t} + V_x \frac{\partial T}{\partial x} + V_y \frac{\partial T}{\partial x}\right) = K \frac{\partial^2 T}{\partial x^2} + \eta \dot{\gamma}^2 \quad [84]$$

the shear rate ($\dot{\gamma}$) is express as:

$$\dot{\gamma} = \left[\left(\frac{\partial v_x}{\partial z}\right)^2 + \left(\frac{\partial v_y}{\partial z}\right)^2\right]^{\frac{1}{2}} \quad [85]$$

From eqn [69], the absolute temperature (T), time (t), melt density (ρ), specific heat of the feedstock (C_p), and K represent thermal conductivity of feedstock. The energy equation for the solid phase is expressed as:

$$\rho_s C_{p_s} \frac{\partial T_s}{\partial t} = K \frac{\partial^2 T_s}{\partial z_s{}^2} \quad [86]$$

where the subscript s represents the solid phase referring to the ceramic or metal powder constituent of the feedstock. Once the governing equations are derived from the continuum-based conservation laws and the constitutive relations, the next task is boundary conditions. A boundary condition for the governing equations involves specification of parameter value(s) and conditions for the filling stage, typically:

Flow equation: melt flow rate at injection point; slip/no slip at cavity wall; free surface at melt front.
Energy equation: melt/injection; temperature at injection point; mold wall temperature; free surface at melt-front.

Note that the boundary conditions are required to solve the governing equation. Therefore, the initial values of the flow rate and injection temperature at the injection node are required. Jiang *et al.*[132] analyzed the feedstock melt and solid phase considering basic assumptions of non-Newtonian and nonisothermal fluid flow.

1.16.4.3.3.5 Packing phase of injection molding

As illustrated in **Figure 8** in Section 1.16.3.2, as the mold cavity filling is nearly completed, the packing phase began. A switchover is experienced as the ram/screw control strategy of the IMM changes from velocity control to pressure control.

Pressure control is required to ensure full filling of the mold cavity and to provide the needed pressure by the filled cavity prior to freezing of the gate. It is important to note that the packing pressure is used to compensate for the anticipated shrinkage in the cooling stage.

In the analysis of the packing stage, it is important to include the effect of melt compressibility. The melt compressibility is dependent on the specific volume of pressure and temperature; this leads to a feedstock-specific PVT relationship/equation state.

Then, suitable PVT and viscosity models are required for the analysis of the packing stage based on the continuum approach; the governing equations are presented as follows.

Mass conservation of the feedstock is expressed as:

$$\frac{\partial \rho}{\partial t} + \frac{\partial(\rho V_x)}{\partial x} + \frac{\partial(\rho V_y)}{\partial y} + \frac{\partial(\rho V_z)}{\partial z} = 0 \quad [87]$$

Assuming that pressure convection terms are ignored in the packing stage, then eqn [87] becomes:

$$K\frac{\partial \rho}{\partial t} - \beta\left(\frac{\partial T}{\partial t} + V_x\frac{\partial T}{\partial x} + V_y\frac{\partial T}{\partial y}\right) + \left(\frac{\partial V_x}{\partial x} + \frac{\partial V_y}{\partial y}\right) = 0 \qquad [88]$$

Where K is the isothermal compressibility coefficient of the material. The energy equation for this processing stage is expressed as:

$$\rho C_p\left(\frac{\partial T}{\partial t} + V_x\frac{\partial T}{\partial x} + V_y\frac{\partial T}{\partial y}\right) = K\frac{\partial^2 T}{\partial x^2} + \eta\dot{\gamma}^2 + \beta T\frac{\partial P}{\partial t} \qquad [89]$$

To replicate the physical model, the same value of shear rate is used for both packing and mold cavity filling, respectively. Typical boundary and initial conditions for the packing analysis stage of IM is presented as follows:

- mass and momentum conservations: specified pressure at injection point, slip condition at cavity wall, and free surface at melt-front.
- energy equation: specified temperature at injection point, mold wall temperature condition at the cavity wall, and free surface at melt-front.
- initial conditions: pressure, velocity, temperature, and density from the results of the filling stage analysis are used.

1.16.4.3.3.6 Cooling phase of injection molding

Mold filling and other preceding processes significantly contribute to the quality of the molded part, but the successful completion of the cooling stage enhances the productivity and the quality of the final component. Cooling starts immediately upon injection of the melt into the mold cavity; theoretically, cooling time is referred to as the period that elapses between when the gate freezes and part ejection.

In the cooling analysis of the mold, the main focus is on the temperature profile at the cavity walls as well as on surface of the mold. The boundary condition will be guided by the melt or filling/injection temperature and the packing phase. When the injection molding process is in the steady state, the mold temperature will fluctuate periodically over time due to the interaction between the hot melt and cavity surface supported by the activities of the cooling medium. Therefore, analysis of the cooling phenomena is investigated to determine the effect of the variant temperature on the molded part. A 3D cycle-averaged approach is adopted for the determination of the cycle-averaged temperature field and its effects on the molded part. This method is chosen to reduce the computation time for the transient component of the thermal analysis of the process. The governing equations of the heat transfer for the injection mold cooling stage based on the cycle-averaged concept is expressed as:

$$\nabla^2\overline{T} = 0 \qquad [90]$$

$$\rho C_p\frac{\partial T}{\partial t} = K\frac{\partial^2 T}{\partial z^2} \qquad [91]$$

Next, specifications of the initial and boundary conditions for the solution of the governing equations are presented. Typically, the initial and boundary conditions for the cooling stage of injection molding are:

- process condition used or specified during packing stage analysis is maintained as initial conditions
- considerations for convective heat transfer associated with the cooling medium, natural convection heat transfer with air, and material properties of the melt and mold.

1.16.4.4 Analytical and Numerical Methods for Injection Molding Simulations

The governing equations are solved using analytical methods, but as the physics of the problem becomes more complex, the use of numerical methods and/or software is implemented. However, FDM, FVM, and FEM[133–135] methods were mostly used for the analysis of melt flow with variant conditions such as isothermal, nonisothermal,[136] and non-Newtonian.[137] Due to the challenges of handling mesh or elements in the aforementioned methods, the use of mesh-free methods[133,138] for the injection molding process is now being investigated. Kim and Turng[139] present a comprehensive review of the developments of 3D CAE simulation for injection molding. The study is aimed at providing insights into the emerging 3D CAE tools to facilitate judicious application and further developments for the design and manufacturing of complex injection molded parts.

1.16.4.5 Process Simulation and Quality Characteristics for Defect-Free Parts in PIM

Process simulations are performed to evaluate quality characteristics of the products at various processing stage of PIM. Simulations are implemented to gain a better understanding of the relationship between processing conditions and part quality, which may be possible by experience alone. This has been the main reason for the development of injection molding simulation. The target goal of setting up simulations in injection molding is outlined in Section 1.16.4.3.

Specifically, simulations are set-up to evaluate the effect of processing conditions on quality characteristics of the product. Some of these response factors or quality characteristics tested are homogeneity of feedstock, mold cavity filling, dimensional, mechanical, surface-finished and microstructural morphological, optical thermal, and electrical properties. Attention is always directed toward finished part quality, which can be broadly classified into two groups: internal properties and external properties. The internal properties that characterized the microstructure of a molded part are the internal stress, molecular weight, degree of crystallization, orientation, spherulite size, and the distribution of fillers and reinforcements. The external properties are the dimension, shape, surface, electrical, optical, and mechanical properties. However, research themes and literature on molded part quality are mostly concerned with the external properties and less on the internal properties of the injection molded parts. Molded part quality is critically influenced by material properties, IMM, part/mold cavity design, and processing conditions. Therefore, research interests are focused on the effects of processing parameters and conditions for improved molded parts. These

investigations include modeling and experimental validation of the simulation and predicted results. Simulation and modeling of microinjection molding have been presented in this chapter. However, it is important to remember that debinding of the polymeric binder is critical and requires extra caution for successful PIM. Therefore, several efforts have been put forth to model and predict the decomposition of the polymeric binder during the debinding process to improve production of defect-free parts. Based on the free decomposition model, the depolymerization of polymeric binder components can be described by first-order reaction kinetics. Shi *et al.*[83] proposed a diffusion-controlled model for predicting the remaining weight fraction of the polymeric binder (h), assuming a linear heating rate (z) is expressed as:

$$h = \exp\left\{\frac{K_0 RT^2 \exp[-E/(RT)]}{ZE}\left[1 - \frac{2RT}{E} + \frac{6(RT)^2}{E^2}\right]\right\} \cdot (t \le t_{\mathrm{db}}) \quad [92]$$

When heating rate is high and temperature is uniform, then the polymeric decomposition within the period is relatively small, especially for metal powders, which are good conductors. An estimate of the remaining polymeric weight fraction (h_{db}) at the debinding temperature (T_{db}) is obtained by substituting T_{db} for T in eqn [92]. However, when ($t > t_{db}$), the remaining weight fraction of the polymer is expressed as:

$$h = h_{\mathrm{db}} \exp\left[-K_0 (t - t_{\mathrm{db}}) \exp\left(-\frac{E}{RT_{\mathrm{db}}}\right)\right] \quad [93]$$

The monomer production rate $\dot{Q}$ based on the volume of the polymer particle is estimated from the relationship:

$$\dot{Q} = \frac{V_p}{V_2}\frac{\mathrm{d}(1-h)}{\mathrm{d}t} = \frac{V_p}{V_2} Kh \quad [94]$$

alternatively expressed as:

$$\dot{Q} = \rho_p V_p K_0 \exp\left(-\frac{E}{RT}\right) \exp\left\{\frac{K_0 RT^2 \exp[-E/(RT)]}{ZE}\left[1 - \frac{2RT}{E} + \frac{6(RT)^2}{E^2}\right]\right\} \quad [95]$$

where ρ_p is the density of the polymer, V_P is the polymer volume fraction, K_o is the specific rate constant, Z is the heating rate, E is the activation energy for thermal degradation, and T is the absolute temperature.

Considering diffusion-controlled decomposition situations, the free decomposition model assumes that the monomer pressure in the polymer has no effect on the decomposition kinetics. Therefore, $\dot{Q}$ is expressed as:

$$\dot{Q} = \frac{V_p}{V_2} Khf = \frac{V_p}{V_2} K(1 - W_1)(1 - a_1) \quad [96]$$

where f is the limiting factor that depends on the activities of the monomer and expressed as:

$$f = 1 - \frac{a_1}{a_e} \quad [97]$$

This expression indicates that the limiting factor depends on the ratio of the activity of the monomer (a_1) to the equilibrium activity, and the depolymerization will go to completion at the debinding temperature even in the presence of monomers. The monomer activity in the aforementioned equation can be calculated using the Flory–Huggins relation expressed as:

$$a_1 = \theta_1 \exp\left[(1 - \theta_1) + x(1 - \theta_1)^2\right] \quad [98]$$

where θ is the volume fraction of monomers in the polymer–monomer solution, and x is an interaction parameter for the polymer–monomer system which also appears later in the free volume theory of diffusion. Alternatively, if the monomer vapor pressure over the polymer–monomer solution, P_1, is known, then the activity of the monomer can be obtained as:

$$a_1 = \frac{P_1}{P_1^0} \quad [99]$$

where P_1^0 is the monomer vapor pressure and can be estimated by the Clausius–Claperon relation expressed as:

$$\ln P_1^0 = -\frac{\Delta H_{\mathrm{vap}}}{RT} + I \quad [100]$$

where H_{vap} is the enthalpy of vaporization, I is a constant, and its value depends on the pressure unit used.

Therefore, the monomer concentration (C) within the undegraded core is estimated by the PDE

$$\frac{\partial C}{\partial t} = \frac{1}{r}\frac{\partial}{\partial r}\left(rD\frac{\partial C}{\partial r}\right) + \dot{Q} \quad [101]$$

where r is the radial distance and D is the diffusion coefficient of the monomer through the powder–polymer suspension. Considering two-phase medium containing polymer and particle, the D is estimated by:

$$D = \left(1 - \frac{3V_c}{\partial r}\right) D_p \quad [102]$$

$$D_p = D_{01}(1 - \theta_1)^2(1 - 2x\theta_1) \exp\left[\frac{W_1 V_1(0) + \zeta(1 - W_1)V_2(0)}{V_{Fh}/\omega}\right] \quad [103]$$

$$D_{01} = D_0 \exp\left(-\frac{E_d}{RT}\right) \quad [104]$$

where D_{01} is the pre-exponential factor, D_0 is a constant, and E_d is the activation energy for monomer diffusion. The subscripts 1 and 2 in eqn [103] denote monomer and polymer, respectively. x is the ratio of critical molar volumes of hopping units of the monomer and the polymer. The average hole free volume per unit mass (V_{FH}) is defined in terms of an overlap factor for free volume (ω), K_{11}, K_{12}, K_{21}, and K_{22} represent free volume parameters, and $(T_g)_1$ and $(T_g)_2$ are the glass transition temperatures of the composites materials, expressed as:

$$\frac{V_{FH}}{\omega} = \frac{K_{11}}{\omega} W_1 \left[K_{21} + T - (T_g)_1\right] + \frac{K_{12}}{\omega}(-W_1)\left[K_{22} + T - (T_g)_2\right] \quad [105]$$

1.16.5 PIM Part Fabrication and Applications

Microfabrication of parts and components can be categorized under three main types: microprecision parts, micropatterned parts, and single microparts.[68] These categories are based on precision, scale, and tolerance limits of the components and fabrication capabilities of the techniques.

1.16.5.1 Fabrication Capabilities of μMIM

Fabrication of 3D hollow[140,141] and movable[142] parts by μMIM is now possible. Attia *et al.*[142] developed a novel framework for fabrication of a moving interface by a powder micromolding process. The fundamental principles and techniques of μMIM machines are utilized in pharmaceutical industries for the production of drugs.[143]

1.16.5.2 Inspection and quality control of MIM products

Application of inspection and quality control techniques to products in MIM enhanced finished part quality and productivity. In general, quality control evaluation techniques can be either destructive or nondestructive.[144] These measures are taken to control product defects at various processing stages of MIM and are supported by statistical quality control.[145] This is to correct production inconsistency and product defects such as short shot, shrinkage, distortion, void, sink mark, weld line, and cracks. MIM involved many processing parameters that are interrelated to one another; hence, the defect identified can be handled in multiple ways. **Table 14** illustrates some common defects, causes, and remedies to improve finished part quality. However, finished part quality is enhanced through effective control and monitoring of the process conditions at different stages.[146] Quality characteristics include homogeneity of the

Table 14 Potential causes and remedies of common defects in MIM

Defects	*Potential causes*	*Remedies*
Flash	Viscosity issue	Increasing feedstock solids loading to improve melt viscosity; introduce high-molecular-weight polymers to improve viscosity of the melt
	Low clamp tonage	Decrease injection pressure as well as pack pressure; use higher tonage machine
	Misalignment of parting line, tooling issue	Ensure tooling is appropriately positioned and clamped, parting line
Incomplete fill	Deficient of molten feedstock into mold cavity	Increase pack pressure, injection speed, melt temperature, mold temperature, and shot size; in addition, increase venting
	Material feeding problem	Decrease back pressure and size of feedstock and regrind; if hygroscopic material is involved, ensure that it dried
Sink mark	Poorly filled part	Increase pack pressure, melt temperature, mold temperature, and back pressure for screw recovery; in addition, increase venting and gate size
Voids	Trapped gas and moisture issue	Increase holding pressure and mold temperature and decrease injection speed; in addition, increase gate size
Weld line and/or wrinkle	Premature solidification of molten feedstock (material)	Increase injection speed, melt temperature, pressure for switchover to pack control
	Gas entrapment	Decrease injection speed and increase venting on runner and part
Shrinkage and/or warpage	Part or component distorts during ejection	Decrease mold temperature and increase cool time; in addition, use improved cooling tools and means
	Pressure gradient in component	Decrease hold pressure
Crack	Part cracking during ejection	Decrease pack pressure and melt temperature and increase mold temperature; in addition polish tool
	Cracking after solvent debinding due to stress	Increase venting and mold temperature, then anneal the finished part

Table 15 Comparison of PIM and other manufacturing process

Characteristics	*PIM*	*Sintering*	*Investment casting*	*Machining*
Density[a] (%)	98	86	100	100
Magnetic force[a] (%)	100	70	95	100
Stress[a] (%)	100	70	100	100
Surface finish (μm)	0.8	1.6	3.2	1.6
Weight (g)	0.1–100	5–2000	30–4500	No limit
Wall thickness (mm)	≥0.3–30	≥1.4	≥2	≥2
Design flexibility	High	Medium	Medium	Low
Shape complexity	High	Low	Medium	High
Production rate	High	High	Low	Medium
Material range	High	High	High	Medium
Dimensional tolerance	Close	Poor	Poor	Poor

[a]These quantities are expressed as a percentage of the actual measurement of the quantity.

feedstock test as well as physical and mechanical properties and microstructure of the molded parts.

Despite part defects encountered during the production process of PIM, the technology still stands out and compares favorably with other processes. Table 15 is a comparison of PIM with sintering, investment casting, and machining based on some selected characteristics.

1.16.5.3 Applications and Market Trend of PIM Products

Increased consumer demand and manufacturing for complex, intricate miniature parts and microdevices were catered to by MIM. Application of injection molding to parts and components fabrication has changed product design significantly across all sectors. PIM has applications in many fields of human life, including electronics industry, mechanical parts, armaments industry, household products, medical appliances, automotive parts, tooling, sporting goods, and many more. Table 16 presents an outline of industries and areas of PIM applications, but the technique still faces some challenges, just like other manufacturing processes. Despite these challenges, there is a brighter indication for PIM application in electronic devices and medical implants.[147]

German [148] conducted a survey of available MIM products by region (North America, Europe, Asia, and the rest of the world [ROW]) for various applications. Findings indicated applications that lead in these regions are medical in North America, automotive in Europe, electronics in Asia, and firearms in ROW. Available records have indicated that MIM is heading toward high-volume production of medical, automotive, electronics, and consumer goods for larger and more sophisticated microproducts.[149]

Table 16 Industrial sectors and areas of PIM applications

Industry	*Applications: parts/components*
Electronics	Printer components Digital cameras Disk drive components Heat sinks Mobile SIM card connectors PIN connectors for mobile phone Mobile phone components
Medical	Orthodontic bracket Orthopedic implants Forceps Surgical equipment Sensor housing implantables Aseptic expandable precision blade
Mechanical	Weaving machine components Welding nozzles Mechanical heat engine components Small transmission parts Lock mechanism Gear wheel for microgear Microfluidic devices
Armaments	Rifle sights Magazine catch Trigger and trigger guard Tocket guidance components Projectile stabilizer fin
Tools	Investment casting core Drill bit inserts Wood cutting bit Machining tools
Automotive	Valves Injection nozzles Transmission parts Airbag components Seat worm gear
Consumer	Jewelry Electric toothbrush microgears Watch components Tea and coffee cups Hair-cutting shears
Sports	Golf club heads Spikes/cleats Bicycle parts Ski bindings

1.16.6 Future Research Outlook

Process development is achieved through systematic innovations, and research investigations of injection molding processes over the years have witnessed remarkable achievements. The process of μ-PIM has been developed in recent years with the objective of making ceramics, metals, and its alloys available through mass production of microparts, components, and microdevices. Competing manufacturing technologies such as sintering, investment casting, or micromachining are often limited concerning processable materials and/or large-scale production capability. The process allows introducing new materials (feedstock) with additional properties such as high-temperature stability, strength, toughness, high precision, and surface finishing, as well as heat conductivity and magnetic properties when subject to life applications. Moreover, comparable to microinjection molding of plastics, biomaterial processing has been developed for μPIM to allow in-process joining of two different metallic materials during the injection molding process and within injection machines.

Process development involved all the processing steps of PIM, from powder selection and feedstock preparation to adjustment of injection molding parameters, debinding, and co-sintering conditions of the metal powders. However, more research is needed to enhance both process and part quality.

Therefore, the future research outlook of injection molding can be summarized as follows:

i. Developments and investigations of new feedstock moldability in terms of the binder composition and the metal powder. Also, the successful implementation of the PIM process, especially the debinding and sintering processes.
ii. Further development of related manufacturing techniques such as two-component micrometal injection molding (2C-μ-MIM), bicomponent, biomaterial, and multimaterial, among many other new processing techniques of injection molding in terms of tooling and quality part are being

investigated. This produces net-shape parts with solid interfaces of either different colors or different materials obtained.

iii. Process integration and development to enhance capability and wider application. This could be integration of mixing mechanism and injection process via rapid prototyping and/or additive manufacturing techniques with μMIM.

iv. Development of improved microinjection system with high precision and control capability over the present custom-made μMIM machine in terms of enhanced speeds and control, and process monitoring for producing defect-free parts.

v. To investigate process conditions as they affect molded part quality. A robust design and formulation of multiobjective optimization frameworks allow multiple quality criteria for μIM. The development of these frameworks is to establish a relationship between process parameters and quality characteristics such as part dimensions, surface finish, and mechanical properties as they affect part quality.

vi. Modeling and simulation have improved microinjection molding processes over the years but are still hindered by a number of challenges. Therefore, development of new suitable software or improvement of the existing software, especially for PIM, is highly recommended.

1.16.7 Conclusions

Modern manufacturing processes adopt nearly net-shape techniques for fabrication of parts and components, which requires a minimum number of processing steps and cost. Micrometal PIM technology as a net-shape microfabrication technique has been widely adopted in the manufacturing of various consumer products and medical and electronics components. In general, μPIM has achieved this over the years due to its advantages, such as:

i. suitability for mass production of various products with minimum production cost and short cycle times;

ii. process and product development of the technology has been improving over the years, with the capability of producing two-material/two-color and movable parts;

iii. ability to process various materials such as polymers, ceramics, and metal powders.

Although μPIM technology has been described as a net-shape microfabrication technique, some challenges are encountered at various processing stages. Powder–binder segregation, short shot, void, sink mark, weld line, cracks, shrinkage, and warpage are some of the defects. Furthermore, difficulties in measuring some material properties and factors, which cannot be easily determined experimentally, are now being investigated by modeling, optimization, and process control to improve the quality of molded parts. Therefore, application of computer simulation has improved the quality of molded parts.

Multimedia

Overview of the production process of fabricating net-shape microparts by the metal injection molding (MIM) technique is illustrated in four video tracks. These video files illustrate the processing steps of the MIM showing powder-binder mixing, injection molding, debinding, and sintering processes (Videos 1–4).

Acknowledgments

The authors acknowledge the financial support of the University of Malaya, 50603 Kuala Lumpur, Malaysia, through the University of Malaya Research Grants (UMRG) (RP020–2012A) and (RP020–2012B). Also worthy of appreciation are the provision of facilities and technical contributions by the faculty members in Engineering at the University of Malaya, as well as the editorial team.

See also: 1.15 Micro Plastic Part Filling Capabilities through Simulation and Experiment: A Case Study on Micro Gear Shape

References

1. Lenz, J.; Enneti, R. K.; Onbattuvelli, V.; Kate, K.; Martin, R.; Atre, S. Powder Injection Molding of Ceramic Engine Components for Transportation. *JOM* **2012**, *64* (3), 388–392.
2. Attia, U. M.; Alcock, J. R. A Review of Micro-Powder Injection Moulding as a Microfabrication Technique. *J. Micromech. Microeng.* **2011**, *21* (4), 043001.
3. Piotter, V.; Bauer, W.; Knitter, R.; Mueller, M.; Mueller, T.; Plewa, K. Powder Injection Moulding of Metallic and Ceramic Micro Parts. *Microsyst. Technol.* **2011**, *17* (2), 251–263.
4. Piotter, V.; Mueller, T.; Plewa, K.; Ritzhaupt-Kleissl, H. J.; Ruh, A.; Hausselt, J. One- and Two-Component Micro Powder Injection Moulding Derived from Thermoplastic Microreplication. *Plastics, Rubber, and Composites* **2010**, *39* (7), 287–292.
5. Ruprecht, R.; Gietzelt, T.; Müller, K.; Piotter, V.; Haußelt, J. Injection Molding of Microstructured Components from Plastics, Metals and Ceramics. *Microsyst. Technol.* **2002**, *8* (4–5), 351–358.
6. Rajabi, J.; Muhamad, N.; Sulong, A. B. Effect of Nano-Sized Powders on Powder Injection Molding: A Review. *Microsyst. Technol.-Micro-and Nanosyst.-Inf. Storage and Process. Syst.* **2012**, *18*, 1941–1961.
7. Pantani, R.; Coccorullo, I.; Speranza, V.; Titomanlio, G. Morphology Evolution During Injection Molding: Effect of Packing Pressure. *Polymer* **2007**, *48* (9), 2778–2790.
8. Sha, B.; Dimov, S.; Griffiths, C.; Packianather, M. S. Micro-Injection Moulding: Factors Affecting the Achievable Aspect Ratios. *Int. J. Adv. Manuf. Technol.* **2006**, *33* (1–2), 147–156.
9. Pantani, R.; Coccorullo, I.; Speranza, V.; Titomanlio, G. Modeling of Morphology Evolution in the Injection Molding Process of Thermoplastic Polymers. *Prog. Polym. Sci.* **2005**, *30* (12), 1185–1222.
10. Zhao, J.; Mayes, R. H.; Chen, G.; Xie, H.; Chan, P. S. Effects of Process Parameters on the Micro Molding Process. *Polym. Eng. Sci.* **2003**, *43* (9), 1542–1554.
11. Rosato, D. V.; Rosato, M. G. *Injection Molding Handbook*; Springer Science & Business Media: New York, NY, 2012.
12. Chang, P.-C.; Hwang, S.-J.; Lee, H.-H.; Huang, D.-Y. Development of an External-Type Microinjection Molding Module for Thermoplastic Polymer. *J. Mater. Process. Technol.* **2007**, *184* (1–3), 163–172.
13. Galomb, D. E. Hand Operated Injection Molding Apparatus; US Patent 8616871 B2, December 31, 2013.
14. Galomb, D. E. Injection Molding Apparatus and Method of Constructing the Injection Molding Apparatus; US Patent 2012/0076879 A1; March 29, 2012.
15. Galomb, D. E. Injection Molding Apparatus and Method of Constructing the Injection Molding Apparatus; US Patent 8,070,469 B2; December 6, 2011.
16. Galomb, D. E. Injection Molding Machine Apparatus and Method of Constructing the Same; US Patent 2008/0031995 A1; February 7, 2008.

17. Pracilio, F. P. Hand Operated Injection Molding Instructional Device; US Patent 213 87; April 23, 1974.
18. Azuddin, M.; Choudhury, I. A.; Taha, Z. Development and Performance Evaluation of a Low-Cost Custom-Made Vertical Injection Molding Machine. *J. Braz. Soc. Mech. Sci. & Eng.* **2015**, *37* (1), 79–86.
19. Michaeli, W.; Spennemann, A. A New Injection Molding Technology for Micro Parts. *J. Polym. Eng.* **2001**, *21* (2–3), 87–98.
20. Michaeli, W.; Spennemann, A.; Gärtner, R. New Plastification Concepts for Micro Injection Moulding. *Microsyst. Technol.* **2002**, *8* (1), 55–57.
21. Enneti, R. K.; Onbattuvelli, V. P.; Atre, S. V. 4 – Powder Binder Formulation and Compound Manufacture in Metal Injection Molding (MIM). In *Handbook of Metal Injection Molding*; Heaney, D. F., Ed.; Woodhead Publishing: Cambridge; Philadelphia, PA; New Delhi, 2012; pp. 64–92.
22. González-Gutiérrez, J.; Stringari, G. B.; Emri, I. Powder Injection Molding of Metal and Ceramic Parts. In *Some Critical Issues for Injection Molding*; Wang, J., Ed.; INTECH Open Access Publisher: Zagreb, 2012; pp. 65–88.
23. Sakai, T.; Kikugawa, K. Part II: Injection Molding Machinery and Systems: Injection Molding Machines, Tools, and Processes. In *Injection Molding*; Kamal, M. R., Isayev, A. L., Shih-Jung Liu, Eds.; Hanser: Berlin, 2009; pp. 71–131.
24. Verbraak, C. P. J. M.; Meijer, H. E. H. Screw Design in Injection Molding. *Polym. Eng. Sci.* **1989**, *29* (7), 479–487.
25. Pessoles, X.; Tournier, C. Automatic Polishing Process of Plastic Injection Molds on a 5-Axis Milling Center. *J. Mater. Process. Technol.* **2009**, *209* (7), 3665–3673.
26. Grandguillaume, L.; Lavernhe, S.; Quinsat, Y.; Tournier, C. Mold Manufacturing Optimization: A Global Approach of Milling and Polishing Processes. *Procedia CIRP* **2015**, *31*, 13–18.
27. Hocheng, H.; Kuo, K. L. Fundamental Study of Ultrasonic Polishing of Mold Steel. *Int. J. Mach. Tool. Manu.* **2002**, *42* (1), 7–13.
28. Choi, J. Y.; Jeong, H. D. A Study on Polishing of Molds using Hydrophilic Fixed Abrasive Pad. *Int. J. Mach. Tool. Manu.* **2004**, *44* (11), 1163–1169.
29. Giboz, J.; Copponnex, T.; Mélé, P. Microinjection Molding of Thermoplastic Polymers: A Review. *J. Micromech. Microeng.* **2007**, *17* (6), R96–R109.
30. Smarslok, B.; German, R. M. Identification of Design Parameters in Metal Powder Injection Molding. *J. Adv. Mater.* **2005**, *37* (4), 3–11.
31. Petzoldt, F. Micro Powder Injection Moulding-Challenges and Opportunities. *Powder Inject. Mould. Int.* **2008**, *2* (1), 37–42.
32. EPMA. *Metal Injection Moulding – A Manufacturing Process for Precision Engineering Components*, 3rd ed.; European Powder Metallurgy Association (EPMA): Shrewsbury, 2013.
33. Heaney, D. F. 3 – Powders for Metal Injection Molding (MIM). In *Handbook of Metal Injection Molding*; Heaney, D. F., Ed.; Woodhead Publishing: Cambridge, 2012; pp. 50–63.
34. Heaney, D.; Zauner, R.; Binet, C.; Cowan, K.; Piemme, J. Variability of Powder Characteristics and Their Effect on Dimensional Variability of Powder Injection Moulded Components. *Powder Metall.* **2004**, *47* (2), 144–149.
35. Hidalgo, J.; Jiménez-Morales, A.; Barriere, T.; Gelin, J. C.; Torralba, J. M. Capillary Rheology Studies of Invar 36 Feedstocks for Powder Injection Moulding. *Powder Technol.* **2015**, *273*, 1–7.
36. Wen, G. A.; Cao, P.; Gabbitas, B.; Zhang, D.; Edmonds, N. Development and Design of Binder Systems for Titanium Metal Injection Molding: An Overview. *Metall. Mater. Trans. A* **2013**, *44A* (3), 1530–1547.
37. Thavanayagam, G.; Pickering, K. L.; Swan, J. E.; Cao, P. Analysis of Rheological Behaviour of Titanium Feedstocks Formulated with a Water-Soluble Binder System for Powder Injection Moulding. *Powder Technol.* **2015**, *269*, 227–232.
38. Bakan, H. I. Injection Moulding of Alumina with Partially Water Soluble Binder System and Solvent Debinding Kinetics. *Mater. Sci. Tech.* **2007**, *23* (7), 787–791.
39. Azmirruddin, M.; Johari, N.; Jabir, M.; Ibrahim, R.; Talib, A. R. A. Analysis of the Rheological Behavior and Stability of Inconel 718 Powder Injection Molding (PIM) Feedstock. *Adv. Mater. Conf. (Amc 2012)* **2014**, *879*, 63–72.
40. Abdoos, H.; Khorsand, H.; Yousefi, A. A. Torque Rheometry and Rheological Analysis of Powder-Polymer Mixture for Aluminum Powder Injection Molding. *Mairan. Polym. J.* **2014**, 745–755.
41. Liu, Z. Y.; Loh, N. H.; Tor, S. B.; Khor, K. A. Characterization of Powder Injection Molding Feedstock. *Mater. Charact.* **2003**, *49* (4), 313–320.
42. Rajabi, J.; Muhamad, N.; Sulong, A. B.; Fayyaz, A.; Raza, M. R. The Effect of Nano-Sized Stainless Steel Powder Addition on Mechanical and Physical Properties of Micro Powder Injection Molded Part. *Mater. Des.* **2014**, *63*, 223–232.
43. Abolhasani, H.; Muhamad, N. A New Starch-Based Binder for Metal Injection Molding. *J. Mater. Process. Technol.* **2010**, 961–968.
44. Setasuwon, P.; Bunchavimonchet, A.; Danchaivijit, S. The Effects of Binder Components in Wax/Oil Systems for Metal Injection Molding. *J. Mater. Process. Technol.* **2008**, *196* (1–3), 94–100.
45. Supriadi, S.; Baek, E. R.; Choi, C. J.; Lee, B. T. Binder System For STS 316 Nanopowder Feedstocks in Micro-Metal Injection Molding. *J. Mater. Process. Technol.* **2007**, 270–273.
46. Shimizu, T.; Kitazima, A.; Nose, M.; Fuchizawa, S.; Sano, T. Production of Large Size Parts by MIM Process. *J. Mater. Process. Technol.* **2001**, *119* (1–3), 199–202.
47. Li, Y.-m.; Liu, X.-q.; Luo, F.-h.; Yue, J.-l. Effects of Surfactant on Properties of MIM Feedstock. *T. Nonferr. Metal. Soc.* **2007**, *17* (1), 1–8.
48. Ani, S. M.; Muchtar, A.; Muhamad, N.; Ghani, J. A. Fabrication of Zirconia-Toughened Alumina Parts by Powder Injection Molding Process: Optimized Processing Parameters. *Ceram. Int.* **2014**, 273–280.
49. Dobrzański, L. A.; Matula, G.; Herranz, G.; Várez, A.; Levenfeld, B.; Torralba, J. M. Metal Injection Moulding of HS12–1–5–5 High-Speed Steel Using a PW-HDPE Based Binder. *J. Mater. Process. Technol.* **2006**, *175* (1–3), 173–178.
50. Moballegh, L.; Morshedian, J.; Esfandeh, M. Copper Injection Molding Using a Thermoplastic Binder Based on Paraffin Wax. *Mater. Lett.* **2005**, *59* (22), 2832–2837.
51. Huang, B.; Liang, S.; Qu, X. The Rheology of Metal Injection Molding. *J. Mater. Process. Technol.* **2003**, *137* (1–3), 132–137.
52. Lin, K.-H. Wear Behavior and Mechanical Performance of Metal Injection Molded Fe–2Ni Sintered Components. *Mater. Des.* **2011**, *32* (3), 1273–1282.
53. Dang, X.-P. General Frameworks for Optimization of Plastic Injection Molding Process Parameters. *Simul. Model. Pract. Th.* **2014**, *41*, 15–27.
54. Lenz, J.; Enneti, R. K.; Park, S. J.; Atre, S. V. Powder Injection Molding Process Design for UAV Engine Components Using Nanoscale Silicon Nitride Powders. *Ceram. Int.* **2014**, *40* (1), 893–900.
55. Sun, S.-H.; Tsai, L.-Z. Development of Virtual Training Platform of Injection Molding Machine Based on VR Technology. *Int. J. Adv. Manuf. Technol.* **2012**, *63* (5–8), 609–620.
56. Zhang, N.; Chu, J. S.; Gilcharist, M. D. In Micro Injection Molding: Characterization of Cavity Filling Process. In *SPE Annual Technical Conference*; Society of Plastics Engineering: Boston, MA, 2011; pp. 2085–2091.
57. Liu, L.; Loh, N. H.; Tay, B. Y.; Tor, S. B.; Yin, H. Q.; Qu, X. H. Preparation and Characterization of Micro Components Fabricated by Micro Powder Injection Molding. *Mater. Charact.* **2011**, *62* (6), 615–620.
58. Li, D.; Hou, H.; Liang, L.; Lee, K. Powder Injection Molding 440c Stainless Steel. *Int. J. Adv. Manuf. Technol.* **2010**, *49* (1–4), 105–110.
59. Okubo, K.; Tanaka, S.; Ito, H. Molding Technology for Improvement on Dimensional Accuracy in Micro Metal Injection Molding. *Microsyst. Technol.* **2009**, *15* (6), 887–892.
60. Demers, V.; Turenne, S.; Scalzo, O. Segregation Measurement of Powder Injection Molding Feedstock Using Thermogravimetric Analysis, Pycnometer Density and Differential Scanning Calorimetry Techniques. *Adv. Powder Technol.* **2015**, *26* (3), 997–1004.
61. Hidalgo, J.; Jiménez-Morales, A.; Barriere, T.; Gelin, J. C.; Torralba, J. M. Water Soluble Invar 36 Feedstock Development For μPIM. *J. Mater. Process. Technol.* **2014**, *214* (2), 436–444.
62. Hanemann, T.; Weber, O. Polymethylmethacrylate/Polyethyleneglycol-Based Partially Water Soluble Binder System for Micro Ceramic Injection Moulding. *Microsyst. Technol.-Micro-and Nanosystems-Information Storage and Processing Systems* **2014**, *20* (1), 51–58.
63. Lobo, H. 8 – Characterization of Feedstock in Metal Injection Molding (MIM). In *Handbook of Metal Injection Molding*; Heaney, D. F., Ed.; Woodhead Publishing: Cambridge, 2012; pp. 183–196.
64. Huang, B. Y.; Liang, S. Q.; Qu, X. H. The Rheology of Metal Injection Molding. *J. Mater. Process. Technol.* **2003**, *137* (1–3), 132–137.
65. Kate, K. H.; Enneti, R. K.; Park, S.-J.; German, R. M.; Atre, S. V. Predicting Powder-Polymer Mixture Properties for PIM Design. *Crit. Rev. Solid. State.* **2014**, *39* (3), 197–214.
66. Xie, L.; Shen, L.; Jiang, B. Modelling and Simulation for Micro Injection Molding Process. In *Computational Fluid Dynamics Technologies and Applications*; Minin, I., Ed.; INTECH Open Access Publisher: Croatia, 2011; pp. 317–332.
67. Piotter, V.; Benzler, T.; Gietzelt, T.; Ruprecht, R.; Hausselt, J. Micro Powder Injection Molding. *Adv. Eng. Mater.* **2000**, *2* (10), 639–642.
68. Ruprecht, R.; Finnah, G.; Piotter, V. Microinjection Molding-Principles and Challenges. In *Microengineering of Metals and Ceramics: Part I: Design,*

Tooling and Injection Molding; Baltes, H., Brand, O., Fedder, G. K., Hierold, C., Korvink, J., Tabata, O., Eds.; WILEY-VCH: Germany, 2005; pp. 253–287.
69. Fu, G.; Loh, N. H.; Tor, S. B.; Tay, B. Y.; Murakoshi, Y.; Maeda, R. A Variotherm Mold for Micro Metal Injection Molding. *Microsyst. Technol.-Micro-and Nanosystems-Information Storage and Processing Systems* **2005**, *11* (12), 1267–1271.
70. Kulkarni, S. *Robust Process Development and Scientific Molding: Theory and Practice*; Hanser Publications: Cincinnati, OH, 2010.
71. Surace, R.; Trotta, G.; Fassi, I.; Bellantone, V. The Micro Injection Moulding Process for Polymeric Components Manufacturing. In *New Technologies – Trends, Innovations and Research*; Volosencu, C., Ed.; INTECH Open Access Publisher: Croatia, 2012; pp. 65–90.
72. Enneti, R. K.; Shivashankar, T. S.; Park, S.-J.; German, R. M.; Atre, S. V. Master Debinding Curves for Solvent Extraction of Binders in Powder Injection Molding. *Powder Technol.* **2012**, *228*, 14–17.
73. Krauss, V. A.; Oliveira, A. A. M.; Klein, A. N.; Al-Qureshi, H. A.; Fredel, M. C. A Model for PEG Removal from Alumina Injection Moulded Parts by Solvent Debinding. *J. Mater. Process. Technol.* **2007**, *182* (1–3), 268–273.
74. Enneti, R. K.; Park, S. J.; German, R. M.; Atre, S. V. Review: Thermal Debinding Process in Particulate Materials Processing. *Materials and Manufacturing Processes* **2012**, *27* (2), 103–118.
75. Shengjie, Y.; Lam, Y. C.; Yu, S. C. M.; Tam, K. C. Thermal Debinding Modeling of Mass Transport and Deformation in Powder-Injection Molding Compact. *Metall. Mater. Trans. B* **2002**, *33* (3), 477–488.
76. Li, S. G.; Fu, G.; Reading, I.; *et al.* Dimensional Variation in Production of High-Aspect-Ratio Micro-Pillars Array by Micro Powder Injection Molding. *Appl. Phys. A* **2007**, *89* (3), 721–728.
77. Gorjan, L.; Kosmač, T.; Dakskobler, A. Single-Step Wick-Debinding and Sintering for Powder Injection Molding. *Ceram. Int.* **2014**, *40* (1), 887–891.
78. Md Ani, S.; Muchtar, A.; Muhamad, N.; Ghani, J. A. Binder Removal via a Two-Stage Debinding Process for Ceramic Injection Molding Parts. *Ceram. Int.* **2014**, *40* (2), 2819–2824.
79. Wongpanit, P.; Khanthsri, S.; Puengboonsri, S.; Manonukul, A. Effects of Acrylic Acid-Grafted Hdpe in Hdpe-Based Binder on Properties After Injection and Debinding in Metal Injection Molding. *Mater. Chem. Phys.* **2014**, *147* (1–2), 238–246.
80. Herranz, G.; Levenfeld, B.; Várez, A.; Torralba, J. Development of New Feedstock Formulation Based on High Density Polyethylene for MIM of M2 High Speed Steels. *Powder Metall.* **2005**, *48* (2), 134–138.
81. Aggarwal, G.; Smid, I.; Park, S. J.; German, R. M. Development of Niobium Powder Injection Molding. Part II: Debinding and Sintering. *Int. J. Refract. Metals Hard Mater.* **2007**, *25*, 226–236.
82. Su, H.; Johnson, D. L. Master Sintering Curve: A Practical Approach to Sintering. *J. Am. Ceram. Soc.* **1996**, *79* (12), 3211–3217.
83. Shi, Z.; Guo, Z. X.; Song, J. H. A Diffusion-Controlled Kinetic Model for Binder Burnout in a Powder Compact. *Acta Mater.* **2002**, *50* (8), 1937–1950.
84. Aggarwal, G.; Park, S. J.; Smid, I.; German, R. M. Master Decomposition Curve for Binders Used in Powder Injection Molding. *Metall. Mater. Trans. A* **2007**, *38a* (3), 606–614.
85. German, R. M. *Sintering: From Empirical Observations to Scientific Principles*; Butterworth-Heinemann: New York, NY, 2014.
86. Raza, M. R.; Ahmad, F.; Omar, M. A.; German, R. M. Effects of Cooling Rate on Mechanical Properties and Corrosion Resistance of Vacuum Sintered Powder Injection Molded 316l Stainless Steel. *J. Mater. Process. Technol.* **2012**, *212* (1), 164–170.
87. Choi, J.-P.; Lee, G.-Y.; Song, J.-I.; Lee, W.-S.; Lee, J.-S. Sintering Behavior Of 316l Stainless Steel Micro–Nanopowder Compact Fabricated by Powder Injection Molding. *Powder Technol.* **2015**, *279* (0), 196–202.
88. Shen, C.; Wang, L.; Li, Q. Optimization of Injection Molding Process Parameters Using Combination of Artificial Neural Network and Genetic Algorithm Method. *J. Mater. Process. Technol.* **2007**, *183* (2–3), 412–418.
89. Kurtaran, H.; Erzurumlu, T. Efficient Warpage Optimization of Thin Shell Plastic Parts Using Response Surface Methodology and Genetic Algorithm. *Int. J. Adv. Manuf. Technol.* **2005**, *27* (5–6), 468–472.
90. Yin, F.; Mao, H.; Hua, L. A Hybrid of Back Propagation Neural Network and Genetic Algorithm for Optimization of Injection Molding Process Parameters. *Mater. Des.* **2011**, *32* (6), 3457–3464.
91. Wu, C.-Y.; Ku, C.-C.; Pai, H.-Y. Injection Molding Optimization with Weld Line Design Constraint Using Distributed Multi-Population Genetic Algorithm. *Int. J. Adv. Manuf. Technol.* **2010**, *52* (1–4), 131–141.
92. Shi, H.; Xie, S.; Wang, X. A Warpage Optimization Method for Injection Molding Using Artificial Neural Network with Parametric Sampling Evaluation Strategy. *Int. J. Adv. Manuf. Technol.* **2013**, *65* (1–4), 343–353.
93. Tzeng, C.-J.; Yang, Y.-K.; Lin, Y.-H.; Tsai, C.-H. A Study of Optimization of Injection Molding Process Parameters for SGF and PTFE Reinforced PC Composites Using Neural Network and Response Surface Methodology. *Int. J. Adv. Manuf. Technol.* **2012**, *63* (5–8), 691–704.
94. Shi, H.; Gao, Y.; Wang, X. Optimization of Injection Molding Process Parameters Using Integrated Artificial Neural Network Model and Expected Improvement Function Method. *Int. J. Adv. Manuf. Technol.* **2010**, *48* (9–12), 955–962.
95. Yarlagadda, P. K. D. V. Development of an Integrated Neural Network System for Prediction oProcess Parameters in Metal Injection Moulding. *J. Mater. Process. Technol.* **2002**, *130–131* (0), 315–320.
96. Urval, R.; Lee, S.; Atre, S. V.; Park, S. J.; German, R. M. Optimisation of Process Conditions in Powder Injection Moulding of Microsystem Components Using a Robust Design Method: Part I. Primary Design Parameters. *Powder Metall.* **2008**, *51* (2), 133–142.
97. Khan, Z. A.; Kamaruddin, S.; Siddiquee, A. N. Feasibility Study of Use of Recycled High Density Polyethylene and Multi Response Optimization of Injection Moulding Parameters Using Combined Grey Relational and Principal Component Analyses. *Mater. Des.* **2010**, *31* (6), 2925–2931.
98. Ozcelik, B. Optimization of Injection Parameters for Mechanical Properties of Specimens with Weld Line of Polypropylene Using Taguchi Method. *Int. Commun. Heat. Mass.* **2011**, *38* (8), 1067–1072.
99. Attia, U. M.; Alcock, J. R. Evaluating and Controlling Process Variability in Micro-Injection Moulding. *Int. J. Adv. Manuf. Technol.* **2010**, *52* (1–4), 183–194.
100. Fei, N. C.; Mehat, N. M.; Kamaruddin, S. Practical Applications of Taguchi Method for Optimization of Processing Parameters for Plastic Injection Moulding: A Retrospective Review. *ISRN Ind. Eng.* **2013**, *2013*, 1–11.
101. Attia, U. M.; Alcock, J. R. Optimising Process Conditions for Multiple Quality Criteria in Micro-Injection Moulding. *Int. J. Adv. Manuf. Technol.* **2010**, *50* (5–8), 533–542.
102. Wang, Y.-q.; Kim, J.-g.; Song, J.-i. Optimization of Plastic Injection Molding Process Parameters for Manufacturing a Brake Booster Valve Body. *Mater. Des.* **2014**, *56*, 313–317.
103. Panahi, A. K.; Mianajiy, H.; Miandoabchi, E.; Fareed, M. H. Optimization of the Powder Injection Molding Process Parameters Using the Sequential Simplex Algorithm and Sensitivity Analysis. *J. Manuf. Sci. E-T ASME* **2013**, *135* (1), 1–7.
104. Annicchiarico, D.; Attia, U. M.; Alcock, J. R. A Methodology for Shrinkage Measurement in Micro-Injection Moulding. *Polym. Test.* **2013**, *32* (4), 769–777.
105. Lin, J.; Lian, R.-J. Self-Organizing Fuzzy Controller for Injection Molding Machines. *J. Process. Contr.* **2010**, *20* (5), 585–595.
106. Attia, U.; Marson, S.; Alcock, J. Micro-Injection Moulding of Polymer Microfluidic Devices. *Microfluid. Nanofluid.* **2009**, *7* (1), 1–28.
107. Zhao, P.; Gao, Y.; Zhou, H.; Turng, L. S. Noniterative Optimization Methods. In *Computer Modeling for Injection Molding: Simulation, Optimization, and Control*; Zhou, H., Ed.; John Wiley & Sons: Singapore, 2013; pp. 255–282.
108. Chen, W. C.; Kurniawan, D. Process Parameters Optimization for Multiple Quality Characteristics in Plastic Injection Molding Using Taguchi Method, BPNN, GA, and Hybrid PSO-GA. *Int. J. Precis. Eng. Man.* **2014**, *15* (8), 1583–1593.
109. Mehat, N. M.; Kamaruddin, S. Multi-Response Optimization of Injection Moulding Processing Parameters Using the Taguchi Method. *Polym.-Plast. Technol.* **2011**, *50* (15), 1519–1526.
110. Peter, K.; Rong, Z., *Flow Analysis of Injection Molds*, 2nd ed.; Carl Hanser Verlag GmbH & Co. KG: München, 2013.
111. Zheng, R.; Fan, X.-J.; Tanner, R. I. Injection Molding Integration of Theory and Modeling Methods; Springer Science & Business Media: Germany, 2011.
112. Zhou, H. *Computer Modeling for Injection Molding: Simulation, Optimization, and Control*; John Wiley & Sons: Singapore, 2013.
113. Xie, L.; Ziegmann, G. Influence of Processing Parameters on Micro Injection Molded Weld Line Mechanical Properties of Polypropylene (PP). *Microsyst. Technol.* **2009**, *15* (9), 1427–1435.
114. Gou, G.; Xie, P.; Yang, W.; Ding, Y. Online Measurement of Rheological Properties of Polypropylene Based on an Injection Molding Machine to Simulate the Injection-Molding Process. *Polym. Test.* **2011**, *30* (8), 826–832.
115. Tsai, M.-H.; Ou, K.-L.; Huang, C.-F.; *et al.* Study on Micro-Injection Molding of Light Guiding Plate by Numerical Simulation. *Int. Commun. Heat. Mass.* **2008**, *35* (9), 1097–1100.
116. Lin, H.-Y.; Young, W.-B. Analysis of the Filling Capability to the Microstructures in Micro-Injection Molding. *Appl. Math. Model.* **2009**, *33* (9), 3746–3755.

117. Lin, H.-Y.; Chang, C.-H.; Young, W.-B. Experimental and Analytical Study on Filling of Nano Structures in Micro Injection Molding. *Int. Commun. Heat Mass.* **2010**, *37* (10), 1477–1486.
118. Alexandra, R. New Approaches for the Mathematical Model of Injection Technology Processes. *Analele Universitatii Maritime Constanta* **2012**, *13* (18), 159–162.
119. Wang, W.; Li, X.; Han, X. Numerical Simulation and Experimental Verification of the Filling Stage in Injection Molding. *Polym. Eng. Sci.* **2012**, *52* (1), 42–51.
120. Binet, C.; Heaney, D. F.; Spina, R.; Tricarico, L. Experimental and Numerical Analysis of Metal Injection Molded Products. *J. Mater. Process. Technol.* **2005**, *164–165* (0), 1160–1166.
121. Zauner, R.; Binet, C.; Heaney, D. F.; Piemme, J. Variability of Feedstock Viscosity and Its Correlation with Dimensional Variability of Green Powder Injection Moulded Components. *Powder Metall.* **2004**, *47* (2), 151–156.
122. Cross, M. M. Rheology of Non-Newtonian Fluids: A New Flow Equation for Pseudoplastic Systems. *J. Colloid Sci.* **1965**, *20* (5), 417–437.
123. Carreau, P. J. Rheological Equations from Molecular Network Theories. *Trans. Soc. Rheol. (1957–1977)* **1972**, *16* (1), 99–127.
124. Sisko, A. The Flow of Lubricating Greases. *Ind. Eng. Chem.* **1958**, *50* (12), 1789–1792.
125. El Otmani, R.; Zinet, M.; Benhadid, H. Numerical Simulation and Thermal Analysis of the Filling Stage in the Injection Molding Process: Role of the Mold-Polymer Interface. *J. Appl. Polym. Sci* **2011**, *121* (3), 1579–1592.
126. Chhabra, R. P.; Richardson, J. F. *Chapter 1 – Non-Newtonian Fluid Behaviour*; Butterworth-Heinemann: Oxford, 2008. pp. 1–55.
127. Koszkul, J.; Nabialek, J. Viscosity Models in Simulation of the Filling Stage of the Injection Molding Process. *J. Mater. Process. Technol.* **2004**, *157–158*, 183–187.
128. Kim, J.; Ahn, S.; Atre, S. V.; Park, S. J.; Kang, T. G.; German, R. M. Imbalance Filling of Multi-Cavity Tooling during Powder Injection Molding. *Powder Technol.* **2014**, *257*, 124–131.
129. Ahn, S.; Park, S. J.; Lee, S.; Atre, S. V.; German, R. M. Effect of Powders and Binders on Material Properties and Molding Parameters in Iron and Stainless Steel Powder Injection Molding Process. *Powder Technol.* **2009**, 162–169.
130. Huang, A. N.; Kuo, H. P. Developments in the Tools for the Investigation of Mixing in Particulate Systems – A Review. *Adv. Powder Technol.* **2014**, 163–173.
131. Combarros, M.; Feise, H. J.; Zetzener, H.; Kwade, A. Segregation of Particulate Solids: Experiments and DEM Simulations. *Particuology* **2014**, 25–32.
132. Jiang, B.-y.; Zhong, J.; Huang, B.-y.; Qu, X.-h.; Li, Y.-m. Element Modeling of Fem on the Pressure Field in the Powder Injection Mold Filling Process. *J. Mater. Process. Technol.* **2003**, *137* (1–3), 74–77.
133. Liu, Y. J.; Li, X. G.; Huang, Y. G.; Wei, S. S.; Zeng, G. S. Comparison of Rheological Analytic Model with Numerical Simulation in Powder Injection Molding Filling Process. *J. Cent. South. Univ. T.* **2008**, *15*, 51–56.
134. Jiang, S.; Wang, Z.; Zhou, G.; Yang, W. An Implicit Control-Volume Finite Element Method and Its Time Step Strategies for Injection Molding Simulation. *Comput. Chem. Eng.* **2007**, *31* (11), 1407–1418.
135. Hwang, C. J.; Kwon, T. H. A Full 3D Finite Element Analysis of the Powder Injection Molding Filling Process Including Slip Phenomena. *Polym. Eng. Sci.* **2002**, *42* (1), 33–50.
136. Yang, B.; Ouyang, J.; Liu, C.; Li, Q. Simulation of Non-Isothermal Injection Molding for a Non-Newtonian Fluid by Level Set Method. *Chinese J. Chem. Eng.* **2010**, *18* (4), 600–608.
137. Wang, X.; Li, X. Numerical Simulation of Three Dimensional Non-Newtonian Free Surface Flows in Injection Molding Using ALE Finite Element Method. *Finite Elem. Anal. Des.* **2010**, *46* (7), 551–562.
138. Shamekhi, A.; Sadeghy, K. Cavity Flow Simulation of Carreau–Yasuda Non-Newtonian Fluids Using PIM Meshfree Method. *Appl. Math. Model* **2009**, *33* (11), 4131–4145.
139. Kim, S.-W.; Turng, L.-S. Developments of Three-Dimensional Computer-Aided Engineering Simulation for Injection Moulding. *Model. Simul. Mater. SC* **2004**, *12*, S151–S173.
140. Attia, U. M.; Alcock, J. R. Fabrication of Hollow, 3D, Micro-Scale Metallic Structures by Micro-Powder Injection Moulding. *J. Mater. Process. Technol.* **2012**, *212* (10), 2148–2153.
141. Attia, U. M.; Alcock, J. R. Fabrication of Ceramic Micro-Scale Hollow Components by Micro-Powder Injection Moulding. *J. Eur. Ceram. Soc.* **2012**, *32* (6), 1199–1204.
142. Attia, U. M.; Hauata, M.; Walton, I.; Annicchiarico, D.; Alcock, J. R. Creating Movable Interfaces by Micro-Powder Injection Moulding. *J. Mater. Process. Technol.* **2014**, *214* (2), 295–303.
143. Zema, L.; Loreti, G.; Melocchi, A.; Maroni, A.; Gazzaniga, A. Injection Molding and Its Application to Drug Delivery. *J. Control. Release* **2012**, *159* (3), 324–331.
144. Zhao, P.; Zhou, H.; He, Y.; Cai, K.; Fu, J. A Nondestructive Online Method for Monitoring the Injection Molding Process by Collecting and Analyzing Machine Running Data. *Int. J. Adv. Manuf. Technol.* **2014**, *72* (5–8), 765–777.
145. Gasparin, S.; Tosello, G.; Hansen, H. N.; Islam, A. Quality Control and Process Capability Assessment for Injection-Moulded Micro Mechanical Parts. *Int. J. Adv. Manuf. Technol.* **2012**, *66* (9–12), 1295–1303.
146. Barriere, T.; Liu, B.; Gelin, J. C. Determination of the Optimal Process Parameters in Metal Injection Molding from Experiments and Numerical Modeling. *J. Mater. Process. Technol.* **2003**, *143–144*, 636–644.
147. Tuncer, N.; Bram, M.; Laptev, A.; Beck, T.; Moser, A.; Buchkremer, H. P. Study of Metal Injection Molding of Highly Porous Titanium by Physical Modeling and Direct Experiments. *J. Mater. Process. Technol.* **2014**, *214* (7), 1352–1360.
148. German, R. M. Markets Applications, and Financial Aspects of Global Metal Powder Injection Moulding (MIM) Technologies. *Met. Powder Rep.* **2012**, *67* (1), 18–26.
149. German, R. M. PIM Breaks the $1 bn Barrier. *Met. Powder Rep.* **2008**, *63* (3), 8–10.

Relevant Websites

http://www.advancedpowderproducts.com
Advanced Powder Products, Inc. (APP).
http://www.epma.com/
European Powder Metallurgy Association.
http://www.fimmtech.com
Frontier Injection Molding & Material Technologies.
http://www.pim-international.com/
Magazine for the MIM and CIM Industries.
http://www.mimaweb.org/
Metal Injection Molding Association.
http://www.designforpm.net
Resource for designers and engineers about Powder metallurgy & MIM.
http://www.injectionworld.com/
The Global Magazine for Injection Molders.